

Contents lists available at ScienceDirect

Chemosphere

journal homepage: www.elsevier.com/locate/chemosphere





Ultra-short chain fluorocarboxylates exhibit wide ranging reactivity with hydrated electrons

Camille K. Amador ^{a,b}, Daniel J. Van Hoomissen ^a, Jiaoqin Liu ^{a,b}, Timothy J. Strathmann ^{b,**}, Shubham Vyas ^{a,*}

- ^a Department of Chemistry, Colorado School of Mines, Golden, CO, 80401, USA
- b Department of Civil and Environmental Engineering, Colorado School of Mines, Golden, CO, 80401, USA

HIGHLIGHTS

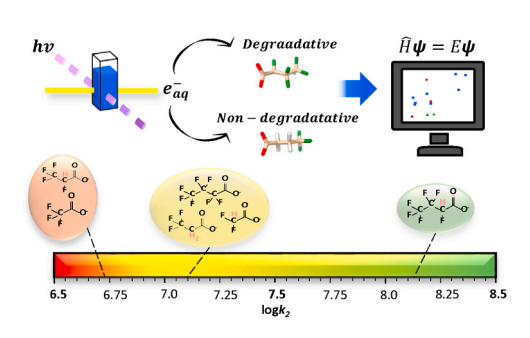
- e_{aq}^- -ARPs show promise in destroying PFAS, but rate constants are lacking.
- LFP was used to measure rate constants of e^-_{aq} reactions with poorly studied PFAS.
- Kinetic values range over two orders of magnitude despite structural similarities.
- ullet DFT provided mechanistic insight into the initial reduction of PFAS by e_{aq}^-
- Non-degradative pathways are possible and pose major concerns for ARP efficiency.

ARTICLE INFO

Handling Editor: Dr Y Yeomin Yoon

Keywords: Laser flash photolysis Rate constant Hydrated electron PFAS Advanced reduction

GRAPHICAL ABSTRACT



ABSTRACT

Recent reports demonstrate that technologies generating hydrated electrons (e_{aq}^- ; e.g., UV-sulfite) are a promising strategy for destruction of per- and polyfluoroalkyl substances, but fundamental rate constants are lacking. This work examines the kinetics and mechanisms of e_{aq}^- reactions with ultra-short chain (C2–C4) fluorocarboxylates using experimental and theoretical approaches. Laser flash photolysis (LFP) was used to measure bimolecular rate constants (k_2 ; M^{-1} s⁻¹) for e_{aq}^- reactions with thirteen per-, and for the first time, polyfluorinated carboxylate structures. The measured k_2 values varied widely from 5.26 \times 10⁶ to 1.30 \times 10⁸ M^{-1} s⁻¹, a large range considering the minor structural changes among the target compounds. Molecular descriptors calculated using density functional theory did not reveal correlation between k_2 values and individual descriptors when considering the whole dataset, however, semiquantitative correlation manifests when grouping by similar possible initial reduction event such as electron attachment at the α -carbon versus β - or γ -carbons along the backbone. From this, it is postulated that fluorocarboxylate reduction by e_{aq}^- occurs via divergent mechanisms with the possibility of non-degradative pathways being prominent. These mechanistic insights provide rationale for contradictory trends between LFP-derived k_2 values and apparent degradation rates recently reported in UV-sulfite constant irradiation treatment experiments.

E-mail addresses: strthmnn@mines.edu (T.J. Strathmann), svyas@mines.edu (S. Vyas).

^{*} Corresponding author.

^{**} Corresponding author.

1. Introduction

Per- and polyfluoroalkyl substances (PFASs) have been used unregulated in many applications for decades (Brennan et al., 2021) but have recently been recognized to be toxic (Barry et al., 2013; Braun et al., 2016; Grandjean et al., 2012), bioaccumulative (Blaine et al., 2013; Rich et al., 2015), and recalcitrant (Moody et al., 2003). Unfortunately, environmental release was already widespread by the time their hazards became well known (Hu et al., 2016; Wang et al., 2014). Treatment of PFAS-contaminated water typically involves physical separation (Appleman et al., 2014; Fabregat-Palau et al., 2022; Franke et al., 2019; Lee et al., 2022; Xiao et al., 2017), but these processes ultimately produce a PFAS-enriched byproduct stream that requires further treatment if destruction is the final objective. As a result, there are growing efforts to study the effectiveness of a range of potential destructive treatment technologies, including electrochemical, plasma, photochemical, and thermochemical processes (Hao et al., 2021; Moriwaki et al., 2005; Sahu et al., 2018; Zhang et al., 2015; Zhuo et al., 2011). One group of technologies of interest are advanced reduction processes (ARPs) based on the photochemical generation of hydrated electrons (e_{aa}^-), a transient species with low reduction potential (-2.9 V) and strong nucleophilic character (Baxendale, 1964; Marcus, 1965). Recently, many reports have focused on treatment of PFASs and other persistent organic pollutants with e_{aq}^- generated by photo-detachment from sulfite (SO₃²) upon excitation with common UV light sources, although other sensitizers have been investigated as well (DiMento et al., 2022; Gu et al., 2017; Jiao et al., 2022; Song et al., 2013). From a practical standpoint, e_{aa}^- based technologies are promising because, unlike oxidative hydroxyl radicals, the reactive species is not inhibited by the presence of many ubiquitous constituents in natural water sources such as chloride, phosphate, and hydroxide (Ren et al., 2021). In addition, the autoxidation of sulfite ions in solution acts to scavenge dissolved oxygen, an efficient e_{aa}^- quencher (1.9 × 10¹⁰ M⁻¹s⁻¹) (Buxton et al., 1988), facilitative for application to water sources that are initially oxic (Hayon et al., 1972; Li et al., 2014). In fact, Liu et al. demonstrated >90% PFAS destruction in a pilot treatment study where no efforts were made to remove dissolved oxygen from the groundwater prior to UV-sulfite treatment (Liu et al., 2021).

While reports of UV-sulfite and other UV-based technologies for e^-_{aq} generation have shown promise for treatment of PFAS-contaminated water, these studies have largely been limited to measuring apparent rates of degradation for target PFASs under constant UV irradiation conditions where the identity and concentrations of transient reactive species, including e^-_{aq} , are unknown (Tenorio et al., 2020). While these studies provide valuable information needed for further technology development, comparison among different experimental systems and prediction of treatment efficacy in new environments remains challenging due to a lack of absolute rate constants and a comprehensive photochemical model for generation and reaction of e^-_{aq} .

Laser flash photolysis (LFP) is a method for studying the reactions of short-lived reactive species (i.e., $ns - \mu s$ lifetimes), such as e_{aq}^- , providing direct kinetic measurements of reactions with target analytes like PFASs while eliminating other adventitious reactions downstream of the initial reduction event. To our knowledge, there are only three previous reports of k_2 measurements for e_{aq}^- reactions with PFASs (Anbar and Hart, 1965; Huang et al., 2007; Maza et al., 2021) and these are limited to fully fluorinated perfluoroalkyl acid structures. There are no reports for reactions with partially fluorinated structures despite the growing recognition of their abundance in many sources of PFAS contamination such as aqueous film forming foams (AFFF) (Ruyle et al., 2021) and the environment (Ghisi et al., 2019). Moreover, there are major discrepancies among these earlier reports. For example, while earlier reports by Huang et al. and Anbar et al. measured k_2 values ranging from 2.3 to 3.4 \times 10⁶ M⁻¹ s⁻¹ for trifluoroacetate (TFA) and 1.3 \times 10⁷ M⁻¹ s⁻¹ for

perfluorobutanoate (PFBA), a more recent study by Maza and coworkers reported k_2 values for TFA (5.0 \times 10⁸ M⁻¹s⁻¹) and PFBA (5.4 \times 10⁸ M⁻¹s⁻¹) that are orders of magnitude greater (Anbar and Hart, 1965; Huang et al., 2007; Maza et al., 2021). This large discrepancy highlights the need for additional studies to confirm k_2 values for these structures and to extend the approach to a broader range of both per- and polyfluorinated structures.

Parent compound decay profiles, which are often used to assess the efficacy of ARPs, are highly sensitive to rate constant, and so accurate k_2 values will be key in modeling these processes in different environments. Here, we report on the application of LFP to directly measure k_2 values for e_{aq}^- reacting with thirteen ultra-short chain (C2-C4) fluorocarboxylate structures including fully and partially fluorinated structures, the latter of which has never been measured before. To date, most studies have focused on e_{aq}^- based treatment of longer-chain perfluoroal kyl acids and much less has been reported on ultra-short chain structures despite recent trends wherein manufacturers are substituting shorter chain analogues for legacy PFASs such as perfluorooctanoic acid (PFOA) and perfluorooctane sulfonic acid (PFOS) (Gordon, 2011; Sun et al., 2016). Since LFP measurements occur on an extremely short timescale, results can be taken as a "snapshot" of the initial reduction events absent of nontarget pathways that might contribute to variable results observed during long-term (e.g., hours or days) UV irradiation experiments. Kinetic parameters and reactivity trends are compared with previous reports from LFP and constant irradiation methods highlighting both similarities and discrepancies among available reports. Variation in k_2 values among the fluorocarboxylates measured here are also analyzed in relation to molecular property descriptors calculated with density functional theory (DFT). The experimental data presented herein alongside computations of molecular property descriptors warrants an extensive computational study on the impact that structural changes of PFAS have on reductive degradation mechanisms. Analysis of the resulting trends are suggestive of divergent rate-determining pathways for e_{aa}^- consumption which has consequence in the design and implementation of ARPs for PFAS treatment.

2. Materials and methods

2.1. Reagents and Solutions

A full list of chemical reagents is provided in the Supporting Information (SI). All stock solutions and reaction samples for LFP experiments were prepared inside an anaerobic chamber (Coy Lab Products; 97% N_2 , 3% H_2) using deoxygenated water prepared as described in SI. Samples prepared in quartz cuvette cells (1 \times 1 cm) were capped and sealed with parafilm before removing from the anaerobic chamber to prevent oxygen exposure during LFP measurements

2.2. Laser flash photolysis setup and procedure

A Nd:YAG laser (Surelite EX, Continuum) operating at 1064 nm with a 10 Hz repetition rate and 4 ns time resolution was used with a 4th harmonic generator to produce 266 nm light. Transient absorbance spectra were collected using LP980 spectrophotometer (Edinburgh Instruments) equipped with ICCD camera and photomultiplier tube. The transient species, e_{aq}^- , was produced by irradiating a mixture of 40 μ M K₄Fe(CN)₆ and 10 μ M K₃Fe(CN)₆ with an 8–10 mJ laser pulse. Decay of e_{aq}^- was monitored by tracking the change in absorbance of its characteristic peak ($\varepsilon=205,560~{\rm M}^{-1}~{\rm cm}^{-1}$ at 690 nm) (Abramczyk et al., 1992; Hart, 1964) using ten averages for each of the measurements. Individual cuvettes were amended with varying concentration (0–50 mM) of the target fluorocarboxylate quencher and Stern-Volmer analysis of the change in e_{aq}^- lifetime (τ) was used to determine the k_2 value. Unless otherwise indicated, reaction solutions were buffered at pH 9.2 (borate) and ionic strength was fixed using NaCl. Quenching due to

buffer and electrolyte are expected to be negligible, and 0 mM fluorocarboxylate control samples highlight this point by displaying constant e_{aa}^- lifetime across experiments (Fig. S1). Additional details of solution conditions and preparation are described in the SI. All samples were prepared and run in triplicate and uncertainties provided represent triplicate-averaged standard deviations. Separate experiments were conducted for selected fluorocarboxylates at pH 12.0 to evaluate the potential influence of solution pH on k_2 . In addition, τ in the absence of fluorocarboxylate quenchers was measured over a range of pH (3.5-12.0) and ionic strength (0-650 mM) values to assess the effects of these variables on background quenching. Due to a change in LFP setup during the course of the study, certain compounds (indicated in Table 1) were measured after exciting the sensitizer with 254 nm laser pulse. This is not expected to affect the measured rate constant values because the absorption spectrum of the sensitizer, K₄Fe(CN)₆, shows strong absorption at all wavelengths <300 nm (Harish et al., 2011), and tests conducted with TFA using both excitation wavelengths yielded similar k_2 values (see Fig. S2).

2.3. Density functional theory calculations

DFT was used to calculate molecular property descriptors for the thirteen target fluorocarboxylate structures that were subjected to LFP measurements. Stationary points were located using the density functional wB97-XD with the aug-cc-pVDZ basis sets as implemented in Gaussian 09 software version C.01. This functional was previously shown to successfully calculate the redox potential of PFAAs, making it an appropriate selection for our reaction of interest (Van Hoomissen and Vyas, 2019). In addition, ω B97-XD includes dispersion corrections which are important for modeling the behavior of PFASs. The SMD implicit solvent model was used to simulate an aqueous environment. All fluorocarboxylates were assumed to be in the deprotonated state, the species that predominates at pH conditions used in experiments and e_{aa}^{-} -based treatment applications. The calculated stationary points were characterized as minimum energy structures by computing the second gradients. Several global descriptors along with local properties such as bond dissociation energy (BDE; kcal/mol) and standard reduction potential $(E_s^\circ; V)$ were calculated to use in reactivity and mechanistic analysis. Further description of the global and local molecular property descriptor variables along with equations are summarized in the SI and vide infra.

3. Results and discussion

3.1. Kinetics measurements

LFP kinetic traces collected for e_{aq}^- quenching by perfluorobutanoate (PFBA) are provided in Fig. 1A (traces for all other compounds are provided in the SI). Following excitation, absorbance values at 690 nm, characteristic of e_{aq}^- (Abramczyk et al., 1992; Hart, 1964), decayed on a μ s timescale, and decay was accelerated by addition of increasing concentrations of the PFBA. Exponential fits of the individual traces were carried out to compute the lifetime (τ ; ns) of the transient e_{aq}^- species. The results of replicate transient spectra were found to be highly reproducible, with triplicate-averaged standard deviation values for τ varying by <10% of the average lifetime values. The resulting τ values were analyzed using a Stern-Volmer type relationship (i.e., $1/\tau$ vs. [PFBA]) to derive the value of the apparent bimolecular rate constant (k_2 ; M^{-1} s⁻¹) for e_{aq}^- reaction with PFBA (Fig. 1B). Table 1 summarizes bimolecular rate constants measured here and elsewhere for thirteen C2–C4 fluorocarboxylates and their non-fluorinated analogues.

The influences of pH (3.5–12.0) and ionic strength (0–630 mM) on e_{aq}^- lifetimes in the absence of fluorocarboxylate quenchers are shown in Figure S4A – S4B in SI. It was found that the e_{aq}^- lifetime remained

relatively constant from pH 9.0 to 12.0 but decreased appreciably at pH < 9.0 (Fig. S4A). The decreased lifetime at lower pH conditions can be attributed to increasing concentration $\mathrm{H}^+,$ which reacts with e^-_{aq} at diffusion-limited rates ($k_2 = 2.3 \times 10^{10} \,\mathrm{M}^{-1} \mathrm{s}^{-1}$) (Buxton et al., 1988). At higher pH conditions, this pathway becomes negligible compared to quenching by the solvent H₂O ($k_{obs} = 1.9 \times 10^1 \text{ s}^{-1}$) and the Fe(CN)₆³⁻ $(k_2 = 3.1 \times 10^9 \,\mathrm{M}^{-1} \mathrm{s}^{-1})$ (Buxton et al., 1988) added to the solution. This is supported by observation of nearly identical Stern-Volmer plots for experiments conducted at pH 9.2 and 12.0 (Fig. S4C). This finding of pH invariance is also noteworthy because it contradicts reports that PFAS degradation by UV-sulfite constant irradiation is significantly faster at pH 12.0 (e.g., $t_{1/2} < 1$ h) than at pH 9.5 ($t_{1/2}$ 8–12 h) (Bentel et al., 2020). The likely reason for this lies in how the rates are measured in LFP when compared to constant irradiation experiments. LFP measures the instantaneous reaction of e^-_{aq} with the PFAS whereas constant irradiation experiments measure the net effects of all reactions in the solution on PFAS degradation, which may be impacted by matrix constituents that react with e_{aq}^- in parallel with the target contaminant.

In the absence of the target contaminant (fluorocarboxylate quencher), e_{aa}^- may decay by three mechanisms: (1) reaction with K₃Fe (CN)6, (2) recombination with itself, and (3) reaction with solvent, i.e., water. To ensure changes in e^-_{aa} lifetime could not be attributed to K_3Fe (CN)₆ an excess amount of this species was added to regard this reaction as pseudo first order (10 $\mu M~K_3 Fe(CN)_6$ for photolysis of 40 $\mu M~K_4 Fe$ (CN)₆ with 266 nm light) (Huang et al., 2007). Radical recombination of e_{aa}^- in our kinetics measurements is encumbered by diffusion limitations imparted by the elevated ionic atmosphere (ionic strength; $\mu = 0.63$) (Schmidt and Bartels, 1995). Measurements in the absence of fluorocarboxylate at varying ionic strength show that e^-_{aq} lifetime decreases only when μ increases from dilute conditions to 0.1 then remains relatively constant with further increases (Fig. S4B). In the case where two ions are of the same charge and $\boldsymbol{\mu}$ increases, formation of the encounter pair becomes more facile, resulting in increased quenching of the e_{aa}^- and hence a shorter lifetime due to increased electrostatic shielding that occurs (Chemical Kinetics, 2007). Either way, all experiments with fluorocarboxylates were performed with a fixed μ to ensure that this variable is controlled for. Moreover, rate constants measured for selected fluorocarboxylates in the present study are comparable to those reported previously for the same compounds measured at lower μ and match well when correcting for these difference (vide infra) (Anbar and Hart, 1965; Huang et al., 2007). To further ensure that elevated μ did not affect reported kinetic values, Stern-Volmer analysis of PFBA at $\mu = 0.2$ (lowest attainable value with 50 mM fluorocarboxylate and 40 mM borate buffer) was conducted. Indeed, this value is comparable to that measured at $\mu = 0.63$ (Fig. S4D). Lastly, the rate constant of e_{aa}^- and H₂O has previously been reported to be 19 s⁻¹, which is slow enough to be neglected (Swallow, 1968).

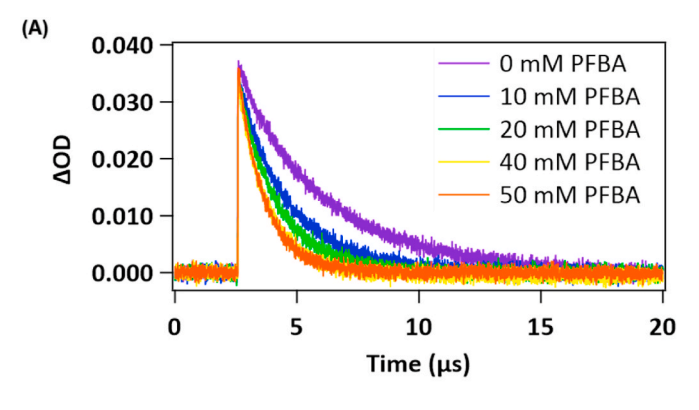
3.2. C2 fluorocarboxylates

Measured k_2 values for ultra-short chain fluorocarboxylates varied widely from 5×10^6 to 1.3×10^8 M $^{-1}$ s $^{-1}$, a large range considering the structural similarities of target compounds. This highlights the sensitivity of e_{aq}^- reactions to small changes in molecular structure of the quenching substrates. Stern-Volmer plots for the three C2 fluoroacetates (TFA, DFA, MFA) are shown in Fig. 2A. The relative reactivity from fastest to slowest [DFA $(1.97\times 10^7~{\rm M}^{-1}~{\rm s}^{-1})>$ MFA $(1.32\times 10^7~{\rm M}^{-1}~{\rm s}^{-1})>$ TFA $(5.26\times 10^6~{\rm M}^{-1}~{\rm s}^{-1})]$ varied \sim 4-fold. In comparison, nonfluorinated acetate exhibits much lower reactivity ($<10^6~{\rm M}^{-1}~{\rm s}^{-1}$) with an uncertainty nearly as large as the value of k_2 measured. Among the C2 – C4 fluorocarboxylates measured in this study, previous reports are only available for TFA and PFBA (Anbar and Hart, 1965; Huang et al., 2007; Maza et al., 2021). The k_2 values measured for these 2 compounds in the present study are similar to values reported by Huang et al.

Table 1 Summary of abbreviations, structures, solutions conditions, and k_2 values of ultra-short chain fluorocarboxylates determined in the current work along with previously reported values. Solution preparation details and kinetics data values can be found in the SI.

Name and Abbreviation	Length	Structure	pH	$\mu \text{ (mol L}^{-1}\text{)}$	This Study k_2 (M ⁻¹ s ⁻¹)	Literature k_2 ($M^{-1}s^{-1}$)
Trifluoroacetate (TFA)	C2	0	9.2	0.63	$(5.26 \pm 0.29) \times 10^{6} \text{ d}$	
		- Ī	12.0	0.63	$(4.16 \pm 0.14) \times 10^6 \text{ d}$	
		F-C	10.0	0.010	,	$(2.3 \pm 0.2) \times 10^6$
		F U	10.0	0.065		$(3.0 \pm 0.2) \times 10^{6}$ a
		' F				$(3.4 \pm 0.3) \times 10^{6}$ a
			10.0	0.10		$(3.4 \pm 0.3) \times 10^{-6}$
			10.0	N/A		$(2.6 \pm 0.6) \times 10^{6}$ b
Difluoroacetate (DFA)	C2	0	10.0	N/A		$(5.0 \pm 1.4) \times 10^{8}$ c
muoroacetate (B171)	62	г н	9.2	0.63	(1.97 \pm 0.04) \times 10^{7} d	
		c c	12.0	0.63	(1.81 \pm 0.03) \times 10^{7} d	
Monofluoroacetate (MFA)	C2	F 0	9.2	0.63	(1.32 \pm 0.05) \times 10^{7} d	
Acetate	C2	H ₂	9.2	0.63	$(8.52 \pm 7.19) \times 10^4$	
		H ₂ C O	9.5–10.5	N/A		(2.0 \pm 0.5) \times 10 6 b
Perfluoropropanoate (PFPrA)	C3	F O	9.2	0.63	$(1.64 \pm 0.08) \times 10^{7}$ d	
		-	12.0	0.63	$(1.38 \pm 0.09) \times 10^{7} \text{ d}$	
		F _ C _ O	10.0	N/A		(5.8 \pm 1.2) \times 10 ^{8 c}
2,3,3,3-tetrafluoropropanoate (2H- PFPrA)	C3	F C H O	9.2	0.63	$(5.58 \pm 0.56) \times 10^6$	
2,2,3,3-tetrafluoropropanoate (3H- PFPrA)	C3	,	9.2	0.63	$\text{(6.17} \pm 0.16\text{)} \times 10^6$	
3,3,3-trifluoropropanoate (TriFPrA)	C3	F F O	9.2	0.63	$(1.28 \pm 0.08) \times 10^7$	
2,2-difluoropropanoate (DiFPrA)	C3	F C O H ₂ O	9.2	0.63	$(1.65 \pm 0.06) \times 10^{7}$	
2-fluoropropanoate (MFPrA)	C3	F F O H ₃ C H O	9.2	0.63	$(6.43 \pm 0.53) \times 10^6$	
Propanoate	C3	F Q	9.2	0.63	$(7.77 \pm 0.44) \times 10^5$	
		H³C C O				
Perfluorobutanoate (PFBA)	C4	''2 F F O	9.2	0.63	$(1.27 \pm 0.06) \times 10^{7} \text{ d}$	
• = •	*	- '≻' Ĭ	12.0	0.63	$(1.29 \pm 0.06) \times 10^{7} \text{ d}$	
			10.0	0.10	(1.2) = 0.00) \(10	(1.3 \pm 0.1) \times 10^{7} a
		F į F į				$(1.3 \pm 0.1) \times 10^{-6}$
		F F F	10.0	N/A		$(5.4 \pm 1.2) \times 10^{8}$ c
H-perfluorobutanoate (2H-PFBA)	C4	F C C C O	9.2	0.63	$(1.32 \pm 0.004) \times 10^8$	
4,4,4-trifluorobutyrate (TriFBA)	C4	F C	9.2	0.63	$(7.35 \pm 0.07) \times 10^7$	
2,2-difluorobutanoate (DiFBA)	C4	F H ₂	9.2	0.63	$(8.81 \pm 0.13) \times 10^7$	
		H ₃ C C C O			•	
Butanoate	C4	H ₂ CCCC	9.2	0.63	$(9.13 \pm 4.09) \times 10^{5}$	

 $[^]a$ From ref (Huang et al., 2007) (LFP at pH 10.0, μ varies, T=25 °C). b From ref (Anbar and Hart, 1965) (Pulse radiolysis in pH 9.5–10.5, μ and T not provided, 0.001 M methanol). c From ref (Maza et al., 2021) (LFP at pH 10.0, μ not provided). d The LFP experiments involving these compounds were performed using 254 nm light, while all others used 266 nm.



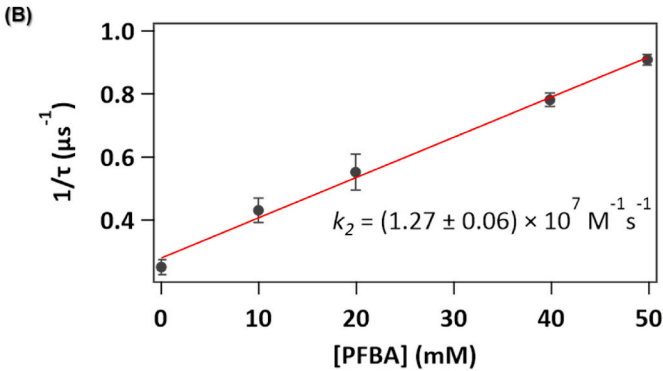
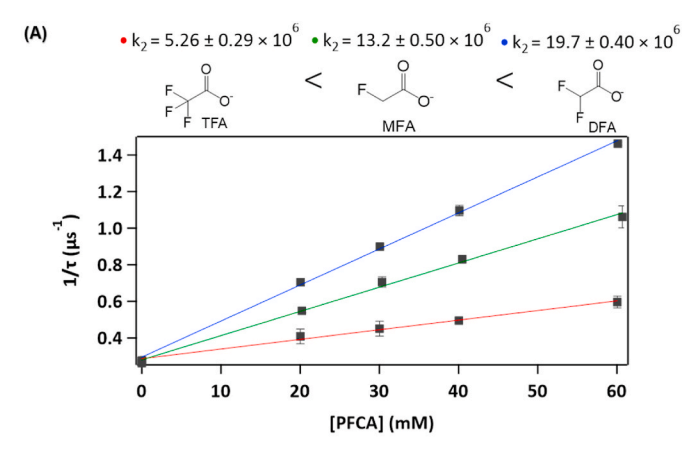


Fig. 1. (A) Kinetic transient absorption traces for e_{aq}^- decay (measured at 690 nm) at pH 9.2 (40 mM borate buffer) in solutions containing 0–50 mM PFBA. Solution conditions: 40 μ M K₄Fe(CN)₆, 10 μ M K₃Fe(CN)₆, ionic strength = 630 mM (balanced using NaCl). (B) Resulting Stern-Volmer plot generated from model fits of the traces to determine e_{aq}^- lifetimes (τ ; μ s) in each solution. Individual kinetic traces in panel (A) represent one of the triplicate measurements, and error bars in panel (B) represent one standard deviation based upon triplicate measurements. Traces and Stern-Volmer plots for all other compounds available in the SI.

 $(2.3-3.4\times10^6~M^{-1}~s^{-1})$ and Anbar et al. $(2.6\times10^6~M^{-1}~s^{-1})$ for TFA and $(1.3\times10^7~M^{-1}~s^{-1})$ for PFBA (Anbar and Hart, 1965; Huang et al., 2007). Huang et al. measured k_2 values for TFA at lower μ (0.01–0.1) than conditions used in the present study, but Fig. 2B shows that linear extrapolation of their values to conditions used in the present study (μ = 0.63) shows an almost perfect match (similar linear extrapolation of data for PFBA shown in Fig. S5).

In comparison, the k_2 value for TFA recently reported by Maza and coworkers (5.0 \times 10⁸ M⁻¹ s⁻¹) is nearly 2 orders-of-magnitude larger than the value measured here as well as values reported in the previous two studies (Maza et al., 2021). While these authors recently posited that the lower k_2 values reported previously may result from aggregation processes occurring at elevated PFAS concentration (Maza et al., 2022) we were unable to measure any appreciable reduction in the lifetime of e_{aq}^- when we added fluorocarboxylate concentrations matching their experiments (i.e., 0.1 mM, see Fig. S6). Furthermore, aggregation of ultra-short chain fluorocarboxylates is much less likely than longer chain fluoroalkyl surfactants. It is hard to rationalize Maza et al.'s k_2 values from a practical standpoint as these values (on the order of 10⁸–10⁹ M⁻¹s⁻¹) would result in much faster degradation kinetics in bulk photolysis UV-ARP experiments. What's more is that both experimental and theoretical studies have found PFSAs to be intrinsically more recalcitrant towards e_{aa}^- reactions than PFCAs (Biswas et al., 2022; Liu et al., 2022), while Maza et al. reports sulfonates to be faster reacting than carboxylates.

While our fluorinated compound data matches the previous work of Huang et al. and Anbar et al., to further validate our measurement



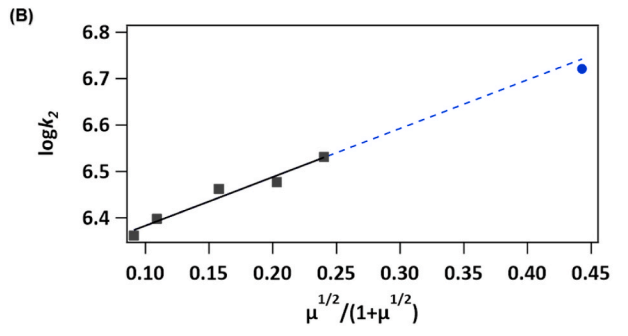


Fig. 2. (A) Stern-Volmer plots for mono-, di-, and trifluoroacetate. Solution conditions are the same as Fig. 1. Units for the k_2 values shown are $M^{-1}s^{-1}$. (B) Influence of solution ionic strength (μ) on k_2 for e_{aq}^- reaction with TFA, including data from the present study (\bullet) and from Huang et al. (\blacksquare) (Huang et al., 2007) Dashed line shows linear extrapolation between the data sets.

protocol, we measured the k_2 values for chloroacetates which revealed much higher reactivity with e_{aq}^- : 1.2×10^9 to 10.3×10^9 M $^{-1}$ s $^{-1}$ (see Fig. S7). This finding is consistent with previous values measured by pulse radiolysis studies $(1.2 \times 10^9$ and 8.5×10^9 M $^{-1}$ s $^{-1}$ for mono- and trichloroacetate, respectively) (Anbar and Hart, 1965), as well as expectations due to the much weaker C–Cl bonds (e.g., 65–85 kcal/mol) (Szwarc and Taylor, 1954) compared to C–F bonds (e.g., 110–130 kcal/mol) (Burdeniuc et al., 1997; Mazurek and Schwarz, 2003). Thus, while chloroacetate species (and presumably bromoand iodo-analogues) react with e_{aq}^- at nearly diffusion-limited rates, comparable fluoroacetate species are much less reactive and will require extended treatment times or higher steady state concentrations of e_{aq}^- in practice.

3.3. C3-C4 fluorocarboxylates

Similar to the C2 structures, the fluorinated C3 and C4 carboxylates were much more reactive with e_{aq}^- than the non-fluorinated analogues. No consistent trends were observed with respect to the effect of complete fluorination on reactivity trends in each group. Although the fully fluorinated TFA (C2) was less reactive than the partially fluorinated analogues, the fully fluorinated propanoate species, perfluoropropanoate (PFPrA), was among the most reactive of the C3 fluorocarboxylates, whereas the fully fluorinated PFBA species was among the least reactive of the C4 fluorocarboxylates. Comparison of the fully fluorinated species shows a reactivity trend of TFA < PFBA < PFPrA, but the overall difference in k_2 values was only a factor of \sim 3. In contrast, much larger variations were observed when one or more F atoms in PFBA are replaced by H atoms. For example, replacement of one F with H at the α -carbon position led to more than a 10-fold increase in k_2 . Interestingly, the same structural change to PFPrA resulted in a 3-fold

decrease in k_2 , whereas replacement of both F on the α -carbon with H had no discernible effect. In general, partial replacement of F with H in the C4 PFBA structure led to large increases in k_2 , whereas similar changes in C3 PFPrA structure had much more limited, and generally negative, effects on k_2 .

3.5. Calculation of molecular properties

Molecular property descriptors for the thirteen fluorocarboxylate target compounds were calculated by DFT (Table S3) to provide insights into the observed trends in measured k_2 values. Important properties calculated include ionization potential (IP; eV), chemical potential (–χ; eV), electron affinity (EA; eV), dipole moment (δ ; debye), and electrophilicity index (ω; eV). Collectively, the large positive IP values and small negative EA values are consistent with molecules in which adding an electron (i.e., reduction) is energetically more favorable than removing an electron (i.e., oxidation). This finding supports a growing body of literature that indicates that PFASs are more amenable towards reduction than oxidation (Bao et al., 2018). The EA values for the perfluorinated structures (TFA, PFPrA, and PFBA) are also more negative than the others in their chain group (C2 vs. C3 vs. C4, respectively), which is to be expected from compounds containing more electron-withdrawing constituents. Additionally, across the whole series of compounds, the C4 molecules have the largest dipole moment (δ) , followed by C3 then C2. This trend follows from the fact that larger molecules can accommodate a larger separation of charge. Further chemical interpretations of select DFT parameters are provided in the SI.

Bond dissociation energy (BDE; kcal/mol) values for individual C-C and C-F bond as well as reduction potential $(E_s^{\circ}; V)$ for each C-F bond were also calculated (Figs. S8 and S9, respectively). As expected, C-F bonds were found to be up to 40 kcal/mol stronger than C-C bonds within the fluorocarboxylate structures. It was also found that BDEs of C–F bonds at the α-carbon were about 110 kcal/mol, while C–F bonds in the middle of the chain were only slightly higher (112 kcal/mol), and C-F bonds at the terminus were significantly higher at about 122 kcal/ mol. In addition, C-C bonds at the terminus were approximately 10 kcal/mol higher than C-C bonds involving the carboxylate headgroup. Reports which calculate molecular properties for ultra-short chain fluorocarboxylates are scarce, however some exist and can be used for comparison. BDE values calculated for the C-F bonds of TriFBA (122.7 kcal/mol) and TFA (116.8 kcal/mol) do agree reasonably well with a recent report by Bentel et al. (124.7 and 119.3 kcal/mol, respectively) (Bentel et al., 2019). The small differences in values likely result from the use of different basis sets and level of theory. E_s° values of C–F bonds show a similar pattern as BDE: C–F bonds attached to the α -carbon are more easily reduced than those at the terminus.

3.6. Relation between bimolecular rate constants and calculated chemical properties

Molecular properties were analyzed against LFP-derived rate constant to assess the correlation between theoretical parameters and experimental values. Fig. 3 shows correlation scatter plots between the $\log k_2$ values and each molecular property descriptor. When considering the full list of 13 compounds, there are no obvious single descriptor correlations (Fig. 3A). One interpretation of this lack of correlation between computed global properties and experimentally determined rate constants is that the fluorocarboxylates considered in this study follow diverging reaction pathways despite limited differences.

For example, correlation may be more obvious when viewing subgroups of the target analytes that are more likely to react with e_{qq}^- by a common mechanism, e.g., just the fully perfluorinated species (i.e., TFA, PFPrA, PFBA; Fig. 3B). There is both experimental and theoretical basis for the notion that e_{qq}^- reduction of perfluorocarboxylates (PFCAs) occurs at the α -carbon resulting in dissociation of an α -fluorine (Biswas et al.,

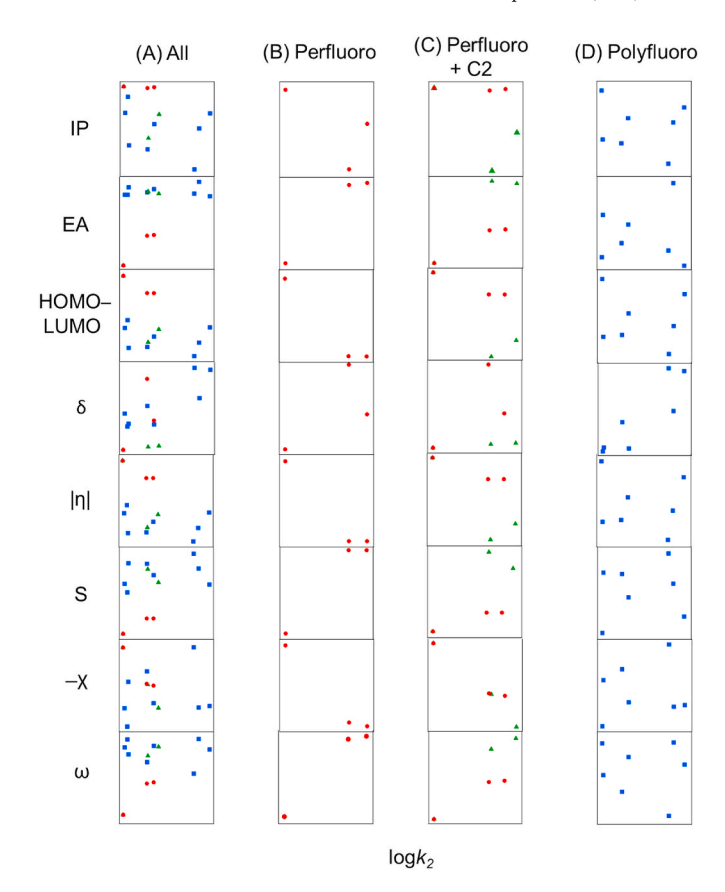


Fig. 3. Scatter correlation plots between measured $\log k_2$ values and DFT-calculated molecular descriptors for (A) all compounds, (B) perfluorinated carboxylates only (\bullet), (C) perfluorinated and C2 carboxylates (\blacktriangle), and (D) polyfluorinated carboxylates only (\blacksquare).

2022; Chen et al., 2019; Van Hoomissen and Vyas, 2019). Focusing on the C2 compounds, a similar rationale of e_{aq}^- attachment and F $^-$ dissociation at the α -position can be made as there are no other C–F positions available (i.e. no β - or γ -positions). Therefore, it is possible that PFCAs and the C2 compounds react via a common mechanism and therefore would correlate more strongly with one or more molecular descriptor (Fig. 3C). While Fig. 3C does show potential correlations with a number of descriptors, particularly for chemical potential ($-\chi$), the small number of analytes in the subgroup prevent more definitive conclusions. The remainder of the dataset includes C3–C4 polyfluorinated carboxylates (Fig. 3D) for which literature on site of e_{aq}^- attachment is not currently available. Inspection of this subgroup exhibits substantial scatter, however, semiquantitative correlation with dipole moment (δ) can be observed. In-depth mechanistic insights of both per- and polyfluorinated carboxylates are provided in the next section.

4. Mechanistic insights

As previously mentioned, there is growing consensus that reduction of fully fluorinated PFCAs is initiated by $e_{\overline{aq}}$ insertion at the α -carbon (Biswas et al., 2022; Chen et al., 2019; Van Hoomissen and Vyas, 2019), but less is established about reduction of partially fluorinated polyfluorinated carboxylates. Three elementary reaction mechanisms which could describe the initiation of fluorocarboxylate reduction by $e_{\overline{aq}}^-$ are concerted, associative, and stepwise cleavage mechanisms, which are described by equations (1)–(3), respectively (Daily and Minakata, 2022)

$$RC - F + e_{aq}^{-} \rightarrow RC^{\bullet} + F^{-} \tag{1}$$

$$RC - F^n + e_{aa}^- \rightarrow [RC - F]^{n-1}$$
 (2)

$$RC - F^n + e_{aa}^- \leftrightarrow [RC - F]^{n-1} \rightarrow RC^{\bullet} + F^-$$
 (3)

Of particular interest are the associative and stepwise reaction mechanisms since concerted pathways are more common in compounds containing weak C-X bonds which are unable to hold the e_{aq}^- (e.g., X=Br and I, depicted in Eq. (1)). Associative mechanisms occur when e_{aq}^- irreversibly reacts with a bond that is strong enough to hold an extra electron (Eq. (2)). This forms an anionic radical species which does not necessarily result in bond cleavage. The stepwise mechanism is initiated by a barrierless, single-electron transfer (SET) step which ensues the formation of an intermediate radical anion (Eq. (3)). This species is resonance stabilized by the π -system of the carboxylate functional group allowing the spin density to eventually accumulate at the site of defluorination and bond cleavage follows (Biswas et al., 2022).

Recently, Daily et al. did an in-depth, thermodynamic study that suggests which mechanism various compounds will undergo upon reaction with e_{aa}^- (Daily and Minakata, 2022). For MFA, TFA, and PFBA, the authors confirm reduction via a stepwise mechanism (PFBA shown below in Scheme 1A for example). While this study did not include C3-C4 polyfluorinated carboxylates, we posit that most of the compounds in our dataset have the functionality to undergo either associative or stepwise mechanisms due to the presence of both strong bonds able to hold an extra electron (associative) and a carboxylate functional group able to stabilize the radical anion species pre-bond cleavage (stepwise). To determine which mechanism each compound is most likely to undergo requires either an exhaustive computational study to obtain E_s° on all possible reaction sites for each mechanism or the use of methods such as ab initio molecular dynamics (AIMD) simulations which are outside the scope of this study. Rather, this study serves to provide accurate rate constants of fluorocarboxylate compounds and highlight potential mechanisms which could prove consequential in implementing e_{aa}^- ARPs in practice.

Two compounds which stand out as not containing functionality to support both mechanisms include the fluorotelomer carboxylic acids (FTCAs) TriFBA and TriFPrA. In FTCAs, the carbon adjacent to the carboxylate headgroup is not fluorinated, and so e_{aq}^- insertion cannot

occur at the α -carbon (recall that e_{aq}^- is unreactive towards acetate, propanoate, and butanoate). Further, a recent study utilizing AIMD simulations reported that upon insertion, e_{aa}^- localizes in specific vicinities in PFAS compounds rather than delocalizing over the entire molecule (Biswas et al., 2022). Therefore, e_{aa}^- insertion and localization in FTCAs occurs at positions other than the α -carbon, so these compounds are unable to impart the same π stabilization as those containing fluorine on the α-carbon. Scheme 1B depicts a hypothetical case in which a FTCA (TriFBA used for example) degrades via the stepwise mechanism. The radical anion formed is unstable (structure ii in Scheme 1B), so this pathway is unlikely to occur. Scheme 1C depicts the alternative case in which a FTCA (TriFBA used again for example) reacts via the associative mechanism. Here, the strong C-F bond of FTCAs holds on to the extra electron without necessarily resulting in cleavage. As a result, fast quenching of the e_{aq}^{-} as measured by LFP (structure ii represented in Scheme 1C) may not reflect the much lower rate at which degradation of the FTCA parent structure occurs (Bentel et al., 2019), i. e., through slower C-F or C-C bond cleavages (potential structure iii in Scheme 1C). We note that the mechanistic insights provided here are focused on elucidating steps involving e_{aq}^- attachment to fluorocarboxylate and those immediately after, not necessarily pathways which could occur downstream of the initial reduction event (i.e., organic radical recombination of, for example, structure iv in Scheme 1A).

As previously mentioned, replacement of F atoms with H atoms in C4 fluorocarboxylates resulted in a stark increase in k_2 value for all substituted compounds. For example, TriFBA was almost 7x more reactive than PFBA. This is counter to trends found in UV-sulfite constant irradiation studies where Bentel et al. reported a half-life for PFBA of approximately 2 h (10 mM sulfite solution buffered at pH 9.5 and irradiated with an 18 W LP Hg light source), whereas TriFBA is only degraded ~10% within 48 h under the same conditions (Bentel et al., 2019). The reason for this inconsistency is attributed to differences in the underlying mechanisms by which each compound reacts with e_{aq}^- . TriFBA is proposed to react via an associative mechanism (rapid uptake of e_{aq}^- , but slow C–F cleavage), whereas PFBA reacts by stepwise mechanism (uptake of e_{aq}^- and subsequent C–F cleavage occur on similar timescales). LFP measures e_{aq}^- quenching explicitly, so it only reflects the

Scheme 1. Proposed mechanism for the initial reduction events involving (A) stepwise C–F bond cleavage for PFBA, (B) stepwise C–F bond cleavage for TriFBA, and (C) associative deactivation of e_{aa}^- for TriFBA. BDEs of bonds of interest are provided in blue in units of kcal/mol.

initial uptake of e_{aq}^- by the fluorocarboxylate substrate. For compounds reacting by stepwise mechanism, this also reflects the rate of fluorocarboxylate degradation, but this may not be the case for compounds reacting by associative mechanism. Constant UV irradiation experiments, on the other hand, measure parent compound decay and therefore reflect compound degradation steps (e.g., C–F cleavage) that may be delayed compared to e_{aq}^- for compounds reacting by associative mechanisms. These findings are critical in that they highlight the plausibility of non-degradative mechanisms in polyfluorinated carboxylates.

5. Conclusions

Hydrated electron (e_{qq}^-) based ARPs are promising for treating recalcitrant pollutants such as PFAS, however, most studies are conducted in constant irradiation systems where only apparent rates of degradation and defluorination are able to be observed. More fundamental parameters, such as bimolecular rate constants (k_2) of e^-_{aa} with target compounds, are critical for evaluating and modeling efficacy of UV-ARPs across various environments. To our knowledge, only three reports in literature have provided k_2 values for the reaction between $e_{aa}^$ and PFAS, and none exist for polyfluorinated compounds. Here, we report k_2 values for thirteen ultra-short chain fluorocarboxylates which will serve as critical inputs in a comprehensive photochemical model for important treatment applications such as UV-sulfite and provide mechanistic insights into the reductive degradation of per- vs. polyfluorinated compounds. Results from this study highlight that subtle structural changes in fluorocarboxylates can yield vast differences in both reduction kinetics and controlling degradation pathways. Calculated molecular descriptors do not show a clear overall trend with observed k_2 values, suggesting the need for more exhaustive dynamic simulation studies to probe the differences in reaction mechanisms. In light of recently proposed possible reaction mechanisms and observed rate constants, it is also recognized that many ubiquitous polyfluorinated structures likely undergo non-degradative mechanisms, posing an additional challenge for treating sites contaminated by diverse PFAS mixtures.

Author contributions

Camille K. Amador: Methodology, investigation, analysis, conceptualization, writing. Daniel J. Van Hoomissen: Conceptualization, methodology. Jiaoqin Liu: Investigation, analysis. Timothy J. Strathmann: Conceptualization, supervision, review, editing. Shubham Vyas: Conceptualization, supervision, review, editing.

Declaration of competing interest

The authors declare that they have no known competing financial interests or personal relationships that could have appeared to influence the work reported in this paper.

Data availability

All supporting data is available as supplementary materials file.

Acknowledgements

This work was financially supported by National Science Foundation (CHE-1807739 and CHE-1710079). The authors also acknowledge the high-performance computing facility at the Colorado School of Mines for allocating computational resources.

Appendix A. Supplementary data

Supplementary data to this article can be found online at https://doi.

org/10.1016/j.chemosphere.2022.136918.

References

- Abramczyk, H., Werner, B., Kroh, J., 1992. Absorption spectra of the solvated electron in hydrocarbons. J. Phys. Chem. 96, 9674–9677. https://doi.org/10.1021/ j.10023c.001
- Anbar, M., Hart, E.J., 1965. The reaction of haloaliphatic compounds with hydrated electrons ¹. J. Phys. Chem. 69, 271–274. https://doi.org/10.1021/j100885a041.
- Appleman, T.D., Higgins, C.P., Quiñones, O., Vanderford, B.J., Kolstad, C., Zeigler-Holady, J.C., Dickenson, E.R.V., 2014. Treatment of poly- and perfluoroalkyl substances in U.S. full-scale water treatment systems. Water Res. 51, 246–255. https://doi.org/10.1016/j.watres.2013.10.067.
- Bao, Y., Deng, S., Jiang, X., Qu, Y., He, Y., Liu, L., Chai, Q., Mumtaz, M., Huang, J., Cagnetta, G., Yu, G., 2018. Degradation of PFOA substitute: GenX (HFPO–da ammonium salt): oxidation with UV/persulfate or reduction with UV/sulfite? Environ. Sci. Technol. acs.est.8b02172. https://doi.org/10.1021/acs.est.8b02172.
- Barry, V., Winquist, A., Steenland, K., 2013. Perfluorooctanoic acid (PFOA) exposures and incident cancers among adults living near a chemical plant. Environ. Health Perspect. 121, 1313–1318. https://doi.org/10.1289/ehp.1306615.
- Baxendale, J.H., 1964. Addendum: redox potential and hydration energy of the hydrated electron. Radiat. Res. Suppl. 4, 139. https://doi.org/10.2307/3583573.
- Bentel, M.J., Liu, Z., Yu, Y., Gao, J., Men, Y., Liu, J., 2020. Enhanced degradation of perfluorocarboxylic acids (PFCAs) by UV/sulfite treatment: reaction mechanisms and system efficiencies at pH 12. Environ. Sci. Technol. Lett. 7, 351–357. https:// doi.org/10.1021/acs.extlett.0c00236.
- Bentel, M.J., Yu, Y., Xu, L., Li, Z., Wong, B.M., Men, Y., Liu, J., 2019. Defluorination of per- and polyfluoroalkyl substances (PFASs) with hydrated electrons: structural dependence and implications to PFAS remediation and management. Environ. Sci. Technol. 53, 3718–3728. https://doi.org/10.1021/acs.est.8b06648.
 Biswas, S., Yamijala, S.S.R.K.C., Wong, B.M., 2022. Degradation of per- and
- Biswas, S., Yamijala, S.S.R.K.C., Wong, B.M., 2022. Degradation of per- and polyfluoroalkyl substances with hydrated electrons: a new mechanism from firstprinciples calculations. Environ. Sci. Technol. 56, 8167–8175. https://doi.org/ 10.1021/acs.est.2c01469.
- Blaine, A.C., Rich, C.D., Hundal, L.S., Lau, C., Mills, M.A., Harris, K.M., Higgins, C.P., 2013. Uptake of perfluoroalkyl acids into edible crops via land applied biosolids: field and greenhouse studies. Environ. Sci. Technol. 47, 14062–14069. https://doi. org/10.1021/es403094q.
- Braun, J.M., Chen, A., Romano, M.E., Calafat, A.M., Webster, G.M., Yolton, K., Lanphear, B.P., 2016. Prenatal perfluoroalkyl substance exposure and child adiposity at 8 years of age: the HOME study: prenatal PFAS Exposure and Child Adiposity. Obesity 24, 231–237. https://doi.org/10.1002/oby.21258.
- Brennan, N.M., Evans, A.T., Fritz, M.K., Peak, S.A., von Holst, H.E., 2021. Trends in the regulation of per- and polyfluoroalkyl substances (PFAS): a scoping review. Int. J. Environ. Res. Publ. Health 18, 10900. https://doi.org/10.3390/jierph182010900.
- Burdeniuc, J., Jedicka, B., Crabtree, R.H., 1997. Recent advances in C–F bond activation. Chem. Ber. 130, 145–154. https://doi.org/10.1002/cber.19971300203.
- Buxton, G.V., Greenstock, C.L., Helman, W.P., Ross, A.B., 1988. Critical Review of rate constants for reactions of hydrated electrons, hydrogen atoms and hydroxyl radicals (OH/O – in Aqueous Solution. J. Phys. Chem. Ref. Data 17, 513–886. https://doi. org/10.1063/1.555805.
- Chemical Kinetics, 2007. Elsevier. https://doi.org/10.1016/B978-0-444-52186-6.
- Chen, Z., Tian, H., Li, H., Li, J., Hong, R., Sheng, F., Wang, C., Gu, C., 2019. Application of surfactant modified montmorillonite with different conformation for phototreatment of perfluorooctanoic acid by hydrated electrons. Chemosphere 235, 1180–1188. https://doi.org/10.1016/j.chemosphere.2019.07.032.
- Daily, R., Minakata, D., 2022. Reactivities of hydrated electrons with organic compounds in aqueous-phase advanced reduction processes. Environ. Sci. Water Res. Technol. 8, 543–574. https://doi.org/10.1039/D1EW00897H.
- DiMento, B.P., Tusei, C.L., Aeppli, C., 2022. Photochemical degradation of short-chain chlorinated paraffins in aqueous solution by hydrated electrons and hydroxyl radicals. Chemosphere 303, 134732. https://doi.org/10.1016/j. chemosphere 2022 134732
- Fabregat-Palau, J., Vidal, M., Rigol, A., 2022. Examining sorption of perfluoroalkyl substances (PFAS) in biochars and other carbon-rich materials. Chemosphere 302, 134733. https://doi.org/10.1016/j.chemosphere.2022.134733.
- Franke, V., McCleaf, P., Lindegren, K., Ahrens, L., 2019. Efficient removal of per- and polyfluoroalkyl substances (PFASs) in drinking water treatment: nanofiltration combined with active carbon or anion exchange. Environ. Sci. Water Res. Technol. 5, 1836–1843. https://doi.org/10.1039/C9EW00286C.
- Ghisi, R., Vamerali, T., Manzetti, S., 2019. Accumulation of perfluorinated alkyl substances (PFAS) in agricultural plants: a review. Environ. Res. 169, 326–341. https://doi.org/10.1016/j.envres.2018.10.023.
- Gordon, S.C., 2011. Toxicological evaluation of ammonium 4,8-dioxa-3H-perfluorononanoate, a new emulsifier to replace ammonium perfluorooctanoate in fluoropolymer manufacturing. Regul. Toxicol. Pharmacol. 59, 64–80. https://doi. org/10.1016/j.yrtph.2010.09.008.
- Grandjean, P., Andersen, E.W., Budtz-Jørgensen, E., Nielsen, F., Mølbak, K., Weihe, P., Heilmann, C., 2012. Serum vaccine antibody concentrations in children exposed to perfluorinated compounds. JAMA 307. https://doi.org/10.1001/jama.2011.2034.
- Gu, Y., Liu, T., Zhang, Q., Dong, W., 2017. Efficient decomposition of perfluorooctanoic acid by a high photon flux UV/sulfite process: kinetics and associated toxicity. Chem. Eng. J. 326, 1125–1133. https://doi.org/10.1016/j.cej.2017.05.156.

- Hao, S., Choi, Y.-J., Wu, B., Higgins, C.P., Deeb, R., Strathmann, T.J., 2021. Hydrothermal alkaline treatment for destruction of per- and polyfluoroalkyl substances in aqueous film-forming foam. Environ. Sci. Technol. 55, 3283–3295. https://doi.org/10.1021/acs.est.0c06906.
- Harish, S., Joseph, J., Phani, K.L.N., 2011. Interaction between gold (III) chloride and potassium hexacyanoferrate (II/III)—does it lead to gold analogue of Prussian blue? Electrochim. Acta 56, 5717–5721. https://doi.org/10.1016/j.electacta.2011.04.044.
- Hart, E.J., 1964. The Hydrated Electron: properties and reactions of this most reactive and elementary of aqueous negative ions are discussed. Science 146, 19–25. https://doi.org/10.1126/science.146.3640.19.
- Hayon, E., Treinin, A., Wilf, J., 1972. Electronic spectra, photochemistry, and autoxidation mechanism of the sulfite-bisulfite-pyrosulfite systems. SO2-, SO3-, SO4-, and SO5- radicals. J. Am. Chem. Soc. 94, 47–57. https://doi.org/10.1021/ ia00756a009.
- Hu, X.C., Andrews, D.Q., Lindstrom, A.B., Bruton, T.A., Schaider, L.A., Grandjean, P., Lohmann, R., Carignan, C.C., Blum, A., Balan, S.A., Higgins, C.P., Sunderland, E.M., 2016. Detection of poly- and perfluoroalkyl substances (PFASs) in U.S. Drinking water linked to industrial sites, military fire training areas, and wastewater treatment plants. Environ. Sci. Technol. Lett. 3, 344–350. https://doi.org/10.1021/acs.estlett.6b00260.
- Huang, L., Dong, W., Hou, H., 2007. Investigation of the reactivity of hydrated electron toward perfluorinated carboxylates by laser flash photolysis. Chem. Phys. Lett. 436, 124–128. https://doi.org/10.1016/j.cplett.2007.01.037.
- Jiao, H., Zhang, C., Yang, M., Wu, Y., Zhou, Q., Hoffmann, M.R., 2022. Photoreductive defluorination of trifluoroacetic acid (TFA) in the aqueous phase by hydrated electrons. Chem. Eng. J. 430, 132724 https://doi.org/10.1016/j.cej.2021.132724.
- Lee, T., Speth, T.F., Nadagouda, M.N., 2022. High-pressure membrane filtration processes for separation of Per- and polyfluoroalkyl substances (PFAS). Chem. Eng. J. 431, 134023 https://doi.org/10.1016/j.cej.2021.134023.
- Li, X., Fang, J., Liu, G., Zhang, S., Pan, B., Ma, J., 2014. Kinetics and efficiency of the hydrated electron-induced dehalogenation by the sulfite/UV process. Water Res. 62, 220–228. https://doi.org/10.1016/j.watres.2014.05.051.
- Liu, C.J., McKay, G., Jiang, D., Tenorio, R., Cath, J.T., Amador, C., Murray, C.C., Brown, J.B., Wright, H.B., Schaefer, C., Higgins, C.P., Bellona, C., Strathmann, T.J., 2021. Pilot-Scale field demonstration of a hybrid nanofiltration and UV-sulfite treatment train for groundwater contaminated by per- and polyfluoroalkyl substances (PFASs). Water Res. 117677 https://doi.org/10.1016/j. wates 2021.117677
- Liu, Z., Chen, Z., Gao, J., Yu, Y., Men, Y., Gu, C., Liu, J., 2022. Accelerated degradation of perfluorosulfonates and perfluorocarboxylates by UV/sulfite + iodide: reaction mechanisms and system efficiencies. Environ. Sci. Technol. 56, 3699–3709. https://doi.org/10.1021/acs.est.1c07608.
- Marcus, R.A., 1965. Theory of electron-transfer reaction rates of solvated electrons. J. Chem. Phys. 43, 3477–3489. https://doi.org/10.1063/1.1696504.
- Maza, W.A., Breslin, V.M., Owrutsky, J.C., Pate, B.B., Epshteyn, A., 2021. Nanosecond transient absorption of hydrated electrons and reduction of linear perfluoroalkyl acids and sulfonates. Environ. Sci. Technol. Lett. 8, 525–530. https://doi.org/ 10.1021/acs.estlett.1c00383
- Maza, W.A., Etz, B.D., Schutt, T.C., Chaloux, B.L., Breslin, V.M., Pate, B.B., Shukla, M.K., Owrutsky, J.C., Epshteyn, A., 2022. Impact of submicellar aggregation on reduction kinetics of perfluorooctanoate by the hydrated electron. Environ. Sci. Technol. Lett. 9, 226–232. https://doi.org/10.1021/acs.estlett.1c01020.
- Mazurek, U., Schwarz, H., 2003. Carbon–fluorine bond activation—looking at and learning from unsolvated systems. Chem. Commun. 1321–1326. https://doi.org/ 10.1039/B211850E.
- Moody, C.A., Hebert, G.N., Strauss, S.H., Field, J.A., 2003. Occurrence and persistence of perfluorooctanesulfonate and other perfluorinated surfactants in groundwater at a fire-training area at Wurtsmith Air Force Base. Michigan. USAElectronic

- supplementary information (ESI) available: map of location of Wurtsmith Air Force Base, Oscoda, MI and surrounding states. J. Environ. Monit. 5, 341–345. https://doi.org/10.1039/b212497a. See. http://www.rsc.org/suppdata/em/b2/b212497a/.
- Moriwaki, H., Takagi, Y., Tanaka, M., Tsuruho, K., Okitsu, K., Maeda, Y., 2005.
 Sonochemical decomposition of perfluorooctane sulfonate and perfluorooctanoic acid. Environ. Sci. Technol. 39, 3388–3392. https://doi.org/10.1021/es040342v.
- Ren, Z., Bergmann, U., Leiviskä, T., 2021. Reductive degradation of perfluorooctanoic acid in complex water matrices by using the UV/sulfite process. Water Res. 205, 117676 https://doi.org/10.1016/j.watres.2021.117676.
- Rich, C.D., Blaine, A.C., Hundal, L., Higgins, C.P., 2015. Bioaccumulation of perfluoroalkyl acids by earthworms (*Eisenia fetida*) exposed to contaminated soils. Environ. Sci. Technol. 49, 881–888. https://doi.org/10.1021/es504152d.
- Ruyle, B.J., Pickard, H.M., LeBlanc, D.R., Tokranov, A.K., Thackray, C.P., Hu, X.C., Vecitis, C.D., Sunderland, E.M., 2021. Isolating the AFFF signature in coastal watersheds using oxidizable PFAS precursors and unexplained organofluorine. Environ. Sci. Technol. 55, 3686–3695. https://doi.org/10.1021/acs.est.0c07296
- Sahu, S.P., Qanbarzadeh, M., Ateia, M., Torkzadeh, H., Maroli, A.S., Cates, E.L., 2018. Rapid degradation and mineralization of perfluorooctanoic acid by a new petitjeanite Bi ₃ O(OH)(PO ₄) ₂ microparticle ultraviolet photocatalyst. Environ. Sci. Technol. Lett. 5, 533–538. https://doi.org/10.1021/acs.estlett.8b00395.
- Schmidt, K.H., Bartels, D.M., 1995. Lack of ionic strength effect in the recombination of hydrated electrons: $(e-)aq + (e-)aq \rightarrow 2(OH-) + H2$. Chem. Phys. 190, 145–152. https://doi.org/10.1016/0301-0104(94)00332-5.
- Song, Z., Tang, H., Wang, N., Zhu, L., 2013. Reductive defluorination of perfluorooctanoic acid by hydrated electrons in a sulfite-mediated UV photochemical system. J. Hazard Mater. 262, 332–338. https://doi.org/10.1016/j. jhazmat.2013.08.059.
- Sun, M., Arevalo, E., Strynar, M., Lindstrom, A., Richardson, M., Kearns, B., Pickett, A., Smith, C., Knappe, D.R.U., 2016. Legacy and emerging perfluoroalkyl substances are important drinking water contaminants in the cape fear river watershed of North Carolina. Environ. Sci. Technol. Lett. 3, 415–419. https://doi.org/10.1021/acs. estlett.6b00398.
- Swallow, A.J., 1968. Recent results from pulse radiolysis. Photochem. Photobiol. 7, 683–694. https://doi.org/10.1111/j.1751-1097.1968.tb08053.x.
- Szwarc, M., Taylor, J.W., 1954. Determination of some carbon-chlorine bond dissociation energies. J. Chem. Phys. 22, 270–274. https://doi.org/10.1063/ 1.1740050
- Tenorio, R., Liu, J., Xiao, X., Maizel, A., Higgins, C.P., Schaefer, C.E., Strathmann, T.J., 2020. Destruction of per- and polyfluoroalkyl substances (PFASs) in aqueous filmforming foam (AFFF) with UV-sulfite photoreductive treatment. Environ. Sci. Technol. 54, 6957–6967. https://doi.org/10.1021/acs.est.0c00961.
- Van Hoomissen, D.J., Vyas, S., 2019. Early events in the reductive dehalogenation of linear perfluoroalkyl substances. Environ. Sci. Technol. Lett. 6, 365–371. https:// doi.org/10.1021/acs.estlett.9b00116.
- Wang, Z., Cousins, I.T., Scheringer, M., Buck, R.C., Hungerbühler, K., 2014. Global emission inventories for C4–C14 perfluoroalkyl carboxylic acid (PFCA) homologues from 1951 to 2030, Part I: production and emissions from quantifiable sources. Environ. Int. 70, 62–75. https://doi.org/10.1016/j.envint.2014.04.013.
- Xiao, X., Ulrich, B.A., Chen, B., Higgins, C.P., 2017. Sorption of poly- and perfluoroalkyl substances (PFASs) relevant to aqueous film-forming foam (AFFF)-Impacted groundwater by biochars and activated carbon. Environ. Sci. Technol. 51, 6342–6351. https://doi.org/10.1021/acs.est.7b00970.
- Zhang, Z., Chen, J.-J., Lyu, X.-J., Yin, H., Sheng, G.-P., 2015. Complete mineralization of perfluorooctanoic acid (PFOA) by γ -irradiation in aqueous solution. Sci. Rep. 4, 7418. https://doi.org/10.1038/srep07418.
- Zhuo, Q., Deng, S., Yang, B., Huang, J., Yu, G., 2011. Efficient electrochemical oxidation of perfluorooctanoate using a Ti/SnO 2 -Sb-Bi anode. Environ. Sci. Technol. 45, 2973–2979. https://doi.org/10.1021/es1024542.

Supporting Information

for

Ultra-Short Chain Fluorocarboxylates Exhibit Wide Ranging Reactivity with Hydrated Electrons

Camille K. Amador, a,b Daniel J. Van Hoomissen, Jiaoqin Liu, A,b Timothy J. Strathmann, Shubham Vyasa*

1Department of Chemistry, Colorado School of Mines, Golden, CO, 80401, USA

2Department of Civil and Environmental Engineering, Colorado School of Mines, Golden, CO, 80401, USA

*strthmnn@mines.edu *svyas@mines.edu

S1 Contents S1. Methods Section pg. S1.1 Reagents S2 S1.2 Solution preparation S2-S3 S1.3 TFA kinetic traces obtained using 254 and 266 nm light sources **S4** S1.4 Density functional theory parameter equations for global properties **S4** S1.5 Density functional theory parameter equations for local properties **S5 S2.** Chemical interpretations of select DFT parameters **S5** S3. Additional Data Section pg. Effects of solution conditions on e_{aq}^- lifetime S3.1 S6 S3.2 $log k_2$ ionic strength extrapolation **S6** Sub-millimolar e_{aq}^- lifetime measurements **S7** S3.3 Stern-Volmer plots for mono-, di-, and trichloroacetate **S7** S3.4 S3.5 Global molecular properties **S8** S3.6 Bond dissociation energy and reduction potential values S9-S10 S3.7 Stern-Volmer plots S11-S14 Optimized ωB97-XD/aug-cc-pVDZ geometries in SMD S3.8 S15-18 **S4.** References S19

S1. Methods

S1.1 Reagents. All chemicals were used as received without further purification. Sodium heptafluorobutyrate (98%); sodium pentafluoropropionate (98%); 4,4,4-trifluorobutyric acid (98%); and 3,3,3-trifluoropropanoic acid (98%) were purchased from Oakwood Chemical. Sodium trifluoroacetate (97%); difluoroacetic acid, sodium salt (97%); sodium monofluoroacetate (99%); and 2H-perfluorobutyric acid (97%) were purchased from abcr. 2,2,3,3-tetrafluoropropanoic acid (95%); 2,2-difluoropropanoic acid (95%); and 2,3,3,3-tetrafluoropropanoic acid (95%) were purchased from Enamine. 2,2-difluorobutanoic acid (97%) was purchased from Aaron Chemicals. 2-fluoropropanoic acid (97%) was purchased from Manchester Organics. Butanoic (≥ 99%) and propanoic (≥99.5%) acid were purchased from Sigma-Aldrich. Glacial acetic acid (99– 100%) was purchased from Macron Fine Chemicals. Potassium ferricyanide (100.2%), sodium chloride (100.5%), and sodium hydroxide (97.5%) were purchased from Fisher Chemical. Sodium borate, tetra (99.5–101.5%) was purchased from Baker & Adamson. Potassium ferrocyanide (101.3%) was purchased from J.T. Baker.

S1.2 Solution Preparation. Deoxygenated water was used to prepare all solutions inside an anaerobic glovebox to eliminate scavenging of e_{aq}^- by oxygen. Briefly, this was prepared by boiling nanopure water for 3 h while stirring and sparging with $N_{2(g)}$. Stock solution concentrations are summarized in **Table S1**. All reactions were performed in the following conditions unless otherwise stated: fifteen separate cuvettes were prepared containing triplicates of 0, 10, 20, 40, and 50 mM quencher along with 40 μM $K_4Fe(CN)_6$, 10 μ M $K_3Fe(CN)_6$ in 40 mM borate buffer at pH 9.2 (25 ml total for each sample). The pH value 9.2 was selected because it is commonly used in hydrated electron treatment studies (Gu et al., 2017; Li et al., 2014; Yu et al., 2018). Borate buffer was chosen because it is known to be unreactive towards the hydrated electron and absorbs negligibly at 254 nm (Hart, 1969; Li et al., 2012). Ionic strength of all solutions was fixed at 0.63 by adding NaCl to balance ionic strength contributions from the quencher and pH buffer. The elevated ionic strength was used to ensure that this variable could be fixed while adding relatively high concentrations of the target quenchers (up to 60 mM for fluorocarboxylates; up to 500 mM for unfluorinated carboxylates). While use of up to 60 mM fluorocarboxylate is beneficial in LFP experiments for determining k_2 values, these elevated concentrations are not required for UV-ARPs in practice. In fact, constant irradiation experiments are often conducted in systems containing ppt - ppb levels of PFAS which are typical of PFAS-contaminated waters (Bentel et al., 2019; Song et al., 2013; Tenorio et al., 2020). We also note that any e_{aq}^- quenching due to added buffer or electrolyte will be accounted for in the fluorocarboxylate blank sample since these concentrations were kept constant in each measurement. This point is highlighted by the data provided in **Figure S1**, which shows that e_{aq}^- lifetime in the absence of added fluorocarboxylate quencher was found to be similar for all measurements done at the same excitation wavelengths, i.e., 254 nm (**Figure S1A**, red) and 266 nm (**Figure S1B**, blue). e_{aq}^- lifetime data for PFBA at pH 9.5 and 12 (Figure S1A) also shows that background quenching at the two different pH conditions are within error of each other.

The 25 ml samples were prepared in 50 ml centrifuge tubes before transferring triplicate 2.75 ml aliquots to quartz cuvettes, capping, and covering with parafilm. Cuvettes were then removed from the glovebox and immediately used in laser flash photolysis experiments. The remaining solution was used to check the pH of the sample before flash photolysis. To ensure pH was constant during reactions, pH was also measured after flash photolysis by pooling solutions from the three replicate cuvettes. For experiments conducted at pH 12, borate buffer was excluded and 1 M NaOH was used to set the pH value.

Table S1. Chemical concentrations of stock solutions used in experiments. a Fluorocarboxylate stock solutions were prepared in deoxygenated water from chemicals containing no organic cosolvent to avoid artifacts such as e_{aq}^{-} reacting with non-target constituents.

Solution	Component	Concentration (mM)
Salt offset	NaCl	500
Potassium ferricyanide	K_3 Fe(CN) ₆	10
Potassium ferrocyanide	$K_4Fe(CN)_6 \bullet 3H_2O$	10
Buffer and electrolyte	$Na_2B_4O_7 \bullet 10H_2O$ NaCl	50 500
Fluorocarboxylates, sodium salt ^a	Various	500
Eluarocarhovulatos, acid forma	Various	500
Fluorocarboxylates, acid form ^a	NaOH	500

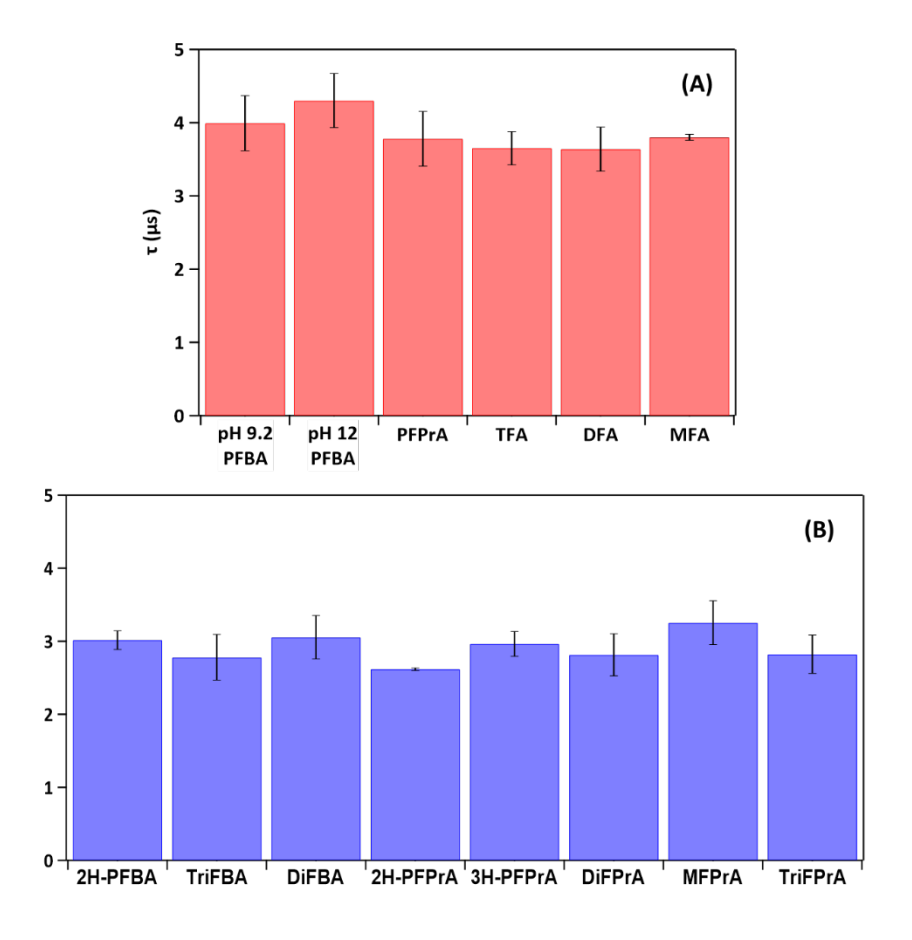


Figure S1. Lifetime of e_{aq}^- in the absence of added fluorocarboxylate quencher (i.e, the 0 mM control samples) using excitation wavelengths: (A) 254 nm and (B) 266 nm.

S1.3 TFA kinetic data obtained using 254 and 266 nm light sources.

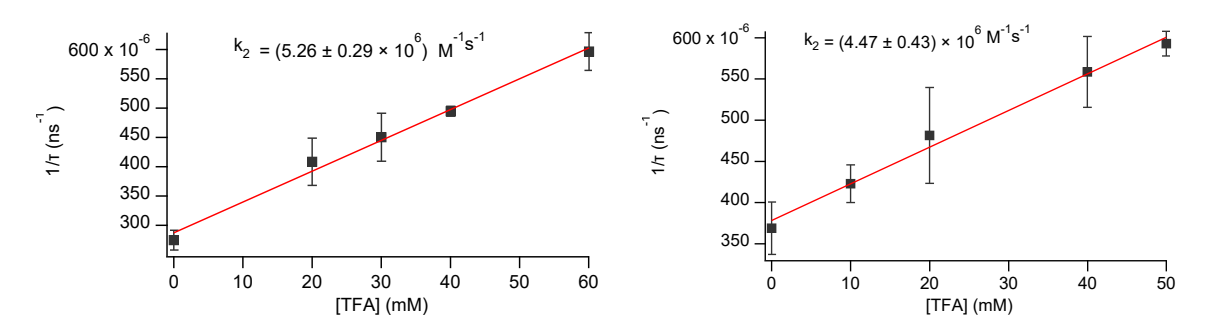


Figure S2. TFA Stern-Volmer plots determined following Fe(CN) $_6$ ⁴⁻ photolysis by 254 nm (left) and 266 nm (right) light. Solutions prepared as described above in **S1.2**. Detailed solution conditions can be found in **Figure 1**.

<u>S1.4 Density functional theory parameter equations for global properties.</u>

Table S2. Equations used to calculate global properties of fluorocarboxylates using DFT-calculated properties.

DFT parameter	Shorthand	Equation	
Ionization Potential	IP	$-E_{HOMO}$	Eq. S1
Electron Affinity	EA	$-E_{LUMO}$	Eq. S2
HOMO-LUMO Gap	Еномо-Ецимо	$E_{HOMO} - E_{LUMO}$	Eq. S3
Dipole	δ	As is	Eq. S4
Hardness	η	$\frac{IP - EA}{2}$	Eq. S5
Softness	S	$\frac{1}{IP - EA}$	Eq. S6
Chemical Potential	-χ	$-\frac{IP + EA}{2}$	Eq. S7
Electrophilicity Index	ω	$\frac{\chi^2}{2\eta}$	Eq. S8

S1.5 Density functional theory equations for global properties. Bond dissociation energies (BDEs) were calculated by taking the difference in enthalpies of the optimized geometries of the products and reactants after breaking each unique C-C and C-F bond, as depicted in **Figure S3**. E_s° was calculated using similar geometries with the calculated Gibbs free energy used in the Nernst equation.

Figure S3. Example calculation of BDE and E_s° of PFBA determined using the ω B97-XD/aug-cc-pVDZ basis set and level of theory. The SMD implicit solvent model to mimic an aqueous solution environment and all PFCAs were taken to be in the anionic state. "H" denotes enthalpy, while G, n, F, and SHE represent Gibbs free energy, number of electrons transferred, Faraday's constant, and the standard hydrogen electrode, respectively.

S2. Chemical interpretations of select DFT parameters.

Chemical interpretations of select DFT parameters are discussed. Only those which are not commonly encountered are considered. Hardness (η) and chemical potential (- χ) both describe chemical changes within a system. While η describes a molecule's resistance to charge transfer (Cárdenas-Jirón et al., 1997), - χ characterizes a molecule's general tendency to form new substances (Chen, 2019). Compounds with small η values can be said to be less resistant towards charge transfer, while those with large - χ can be said to have a greater tendency to react and form a new substance. In both cases, this would conceptually describe a compound amenable to change. The inverse of η is softness (S); a soft molecule could describe one with low (or zero) positive charge, or one that is easily polarizable (Pearson, 1966); consequently, softness describes a molecule's tendency to undergo charge transfer. The last molecular property of interest is electrophilicity index (ω), which measures the electrophilic power of a compound. This could be seen as a molecule ability to "soak up" electrons (Parr et al., 1999). Negative values of ω correspond to a positive change in energy of the system (Δ E > 0) when it "soaks up" electrons. Therefore, less negative values correspond to more favorable charge transfer process.

S3. Additional Data.

S3.1 Effects of solution conditions on e_{aa}^- lifetime. (A) (B) eaq lifetime (ns) Ionic Strength (mM) (C) 900 x 10⁻⁶ (D) 1/T (ns⁻¹) 0.8 **pH 9.2:** $k_2 = (1.27 \pm 0.059) \times 10^7 \, \text{M}^{-1} \, \text{s}^{-1}$ 0.4 **pH 12**: $k_2 = (1.29 \pm 0.059) \times 10^7 \text{ M}^{-1} \text{ s}^{-1}$ [PFBA] (mM) [PFBA] (mM)

Figure S4. Effects of (A) pH and (B) ionic strength on lifetimes of e_{aq}^- in the absence of fluorocarboxylate quenchers, along with comparison of the kinetics of e_{aq}^- reaction with PFBA measured at (C) pH 9.2 and pH 12, and (D) μ = 0.2 and 0.63. Solution conditions are the same as those in **Figure 1**. Ionic strength in (A) kept constant at 0.63 using NaCl. Solution pH in (B) titrated to pH 12 using 1 M NaOH (no buffer). Ionic strength in (C) is 0.63. Solution pH in (D) is 9.2.

S3.2 logk₂ ionic strength extrapolation

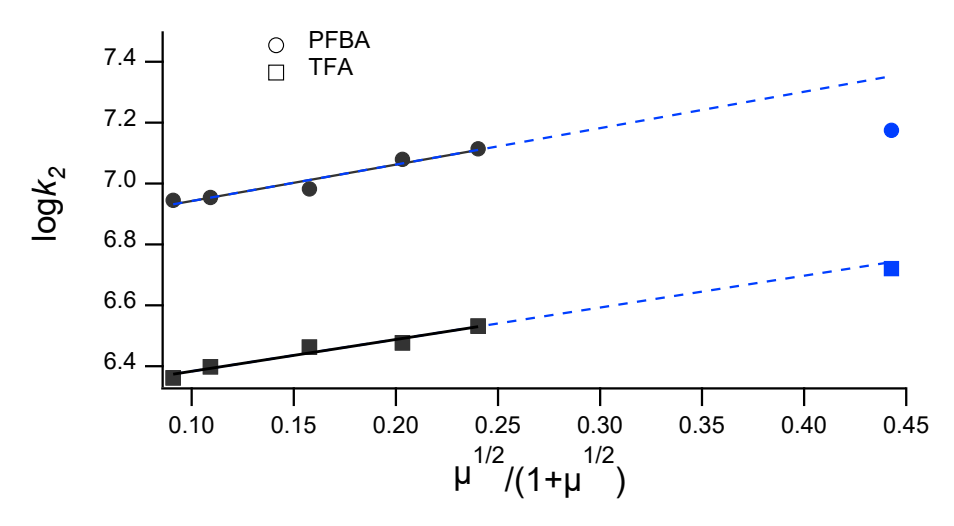


Figure S5. Plots showing influence of ionic strength on measured $log k_2$ values for PFBA and TFA, including data from the present study (blue symbols) and data previously reported by Huang *et al.* (Huang et al., 2007) (black symbols). Dashed blue lines show extrapolation of the trend reported by Huang and co-workers to conditions used in the present study.

S3.3 e_{aq}^{-} lifetime measurements in the presence of sub-millimolar concentrations of various fluorocarboxylates.

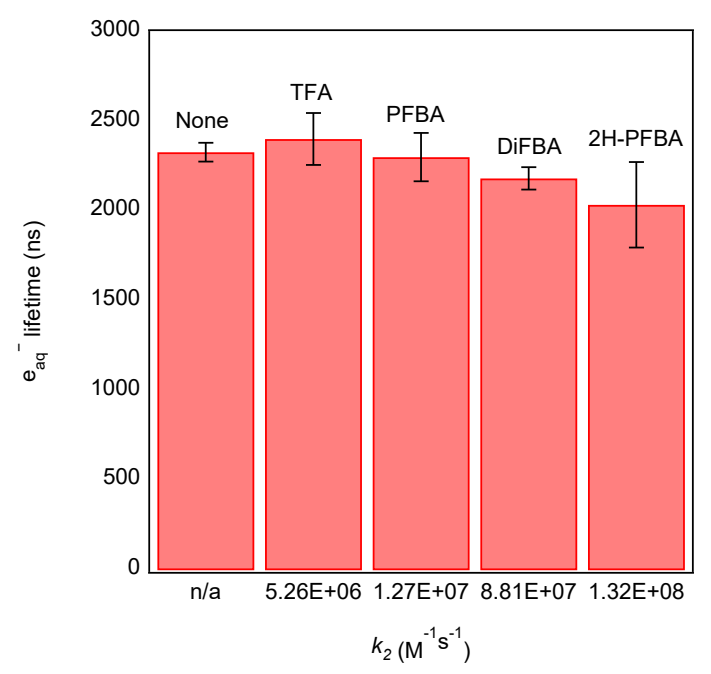


Figure S6. e_{aq}^- lifetime measurements in the absence and presence of various fluorocarboxylates added at a concentration of 0.1 mM. Other solution conditions: 40 μ M K₄Fe(CN)₆, 10 μ M K₃Fe(CN)₆, 40 mM borate buffer, pH 9.2, ionic strength kept constant at 630 mM using NaCl.

S3.4 Stern-Volmer plots for mono-, di-, and trichloroacetate.

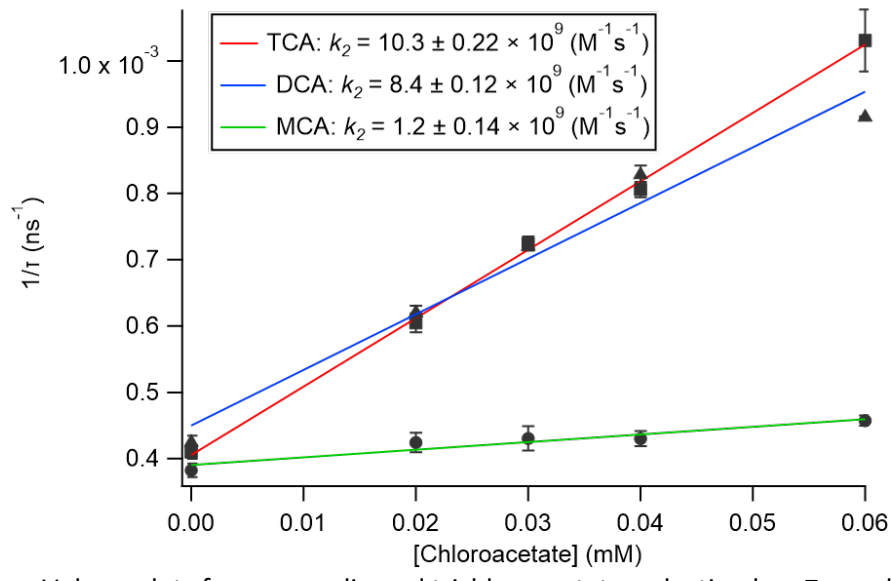


Figure S7. Stern-Volmer plots for mono-, di-, and trichloroacetate reduction by e_{aq}^- produced at similar conditions as those described in **Figure 1**.

S3.5 Global molecular property descriptors.

Table S3. Global molecular properties of fluorocarboxylates in the anionic singlet state calculated by density functional theory.

	•								
No. carbons	Substrate ^a	IP (eV)	EA (eV)		_	η (eV)	S (meV ⁻¹)		ω (eV)
2	TFA	9.73	-2.10	11.8	6.19	5.92	-84.5	-3.812	1.23
	DFA	9.48	-1.37	10.9	6.50	5.43	-92.2	-4.054	1.51
	MFA	9.27	-1.35	10.6	6.42	5.31	-94.2	-3.960	1.48
3	PFPrA	9.72	-1.79	11.5	8.47	5.76	-86.9	-3.964	1.36
	2H-PFPrA	9.49	-1.38	10.9	9.01	5.44	-92.0	-4.055	1.51
	3H-PFPrA	9.64	-1.38	11.0	8.00	5.51	-90.7	-4.128	1.55
	TriFPrA	9.17	-1.36	10.5	9.60	5.26	-95.0	-3.907	1.45
	DiFPrA	9.39	-1.32	10.7	8.16	5.36	-93.3	-4.035	1.52
	MFPrA	9.20	-1.31	10.5	8.22	5.26	-95.1	-3.949	1.48
4	PFBA	9.71	-1.80	11.5	11.7	5.76	-86.8	-3.957	1.36
	2H-PFBA	9.49	-1.40	10.9	12.4	5.44	-91.9	-4.046	1.50
	TriFBA	8.99	-1.37	10.4	12.6	5.18	-96.5	-3.811	1.40
	DiFBA	9.36	-1.25	10.6	10.2	5.30	-94.3	-4.052	1.55
	No. carbons 2	2 TFA DFA MFA 3 PFPrA 2H-PFPrA 3H-PFPrA TriFPrA DiFPrA MFPrA 4 PFBA 2H-PFBA TriFBA	No. carbons Substrate ^a (eV) 2 TFA 9.73 DFA 9.48 MFA 9.27 3 PFPrA 9.72 9.72 2H-PFPrA 9.49 3H-PFPrA 9.64 TriFPrA 9.17 DiFPrA 9.39 MFPrA 9.20 4 PFBA 9.71 2H-PFBA 9.49 TriFBA 8.99	No. carbons Substrate ^a (eV) IP (eV) (eV) 2 TFA 9.73 -2.10 DFA 9.48 -1.37 MFA 9.27 -1.35 3 PFPrA 9.72 -1.79 2H-PFPrA 9.49 -1.38 3H-PFPrA 9.64 -1.38 TriFPrA 9.17 -1.36 DiFPrA 9.39 -1.32 MFPrA 9.20 -1.31 4 PFBA 9.71 -1.80 2H-PFBA 9.49 -1.40 TriFBA 8.99 -1.37	No. carbons Substrate ^a (eV) IP (eV) (eV) (eV) (eV) (eV) EA HOMO— (eV) (eV) 2 TFA 9.73 -2.10 11.8 DFA 9.48 -1.37 10.9 MFA 9.27 -1.35 10.6 3 PFPrA 9.72 -1.79 11.5 2H-PFPrA 9.49 -1.38 10.9 3H-PFPrA 9.64 -1.38 11.0 TriFPrA 9.17 -1.36 10.5 DiFPrA 9.39 -1.32 10.7 MFPrA 9.20 -1.31 10.5 4 PFBA 9.71 -1.80 11.5 2H-PFBA 9.49 -1.40 10.9 TriFBA 8.99 -1.37 10.4	No. carbons Substrate³ IP (eV) EA (eV) HOMO— (eV) (Debye) δ (Debye) 2 TFA 9.73 -2.10 11.8 6.19 DFA 9.48 -1.37 10.9 6.50 MFA 9.27 -1.35 10.6 6.42 3 PFPrA 9.72 -1.79 11.5 8.47 2H-PFPrA 9.49 -1.38 10.9 9.01 3H-PFPrA 9.64 -1.38 11.0 8.00 TriFPrA 9.17 -1.36 10.5 9.60 DiFPrA 9.39 -1.32 10.7 8.16 MFPrA 9.20 -1.31 10.5 8.22 4 PFBA 9.71 -1.80 11.5 11.7 2H-PFBA 9.49 -1.40 10.9 12.4 TriFBA 8.99 -1.37 10.4 12.6	No. carbons Substrate³ IP (eV) (eV) (eV) (eV) (eV) EA LUMO Gap (Debye) (Debye) (eV) (eV) η (eV) (eV) (eV) 2 TFA 9.73 -2.10 11.8 6.19 5.92 DFA 9.48 -1.37 10.9 6.50 5.43 MFA 9.27 -1.35 10.6 6.42 5.31 3 PFPrA 9.72 -1.79 11.5 8.47 5.76 2H-PFPrA 9.49 -1.38 10.9 9.01 5.44 3H-PFPrA 9.64 -1.38 11.0 8.00 5.51 TriFPrA 9.17 -1.36 10.5 9.60 5.26 DiFPrA 9.39 -1.32 10.7 8.16 5.36 MFPrA 9.20 -1.31 10.5 8.22 5.26 4 PFBA 9.71 -1.80 11.5 11.7 5.76 2H-PFBA 9.49 -1.40 10.9 12.4 5.44 TriFBA 8.99 -1.37 <td< td=""><td>No. carbons Substrate^a (eV) IP (eV) (eV) (eV) EA HOMO— (Debye) (eV) (eV) η (eV) (eV) (meV⁻¹) S (meV⁻¹) 2 TFA 9.73 -2.10 11.8 6.19 5.92 -84.5 DFA 9.48 -1.37 10.9 6.50 5.43 -92.2 MFA 9.27 -1.35 10.6 6.42 5.31 -94.2 3 PFPrA 9.72 -1.79 11.5 8.47 5.76 -86.9 2H-PFPrA 9.49 -1.38 10.9 9.01 5.44 -92.0 3H-PFPrA 9.64 -1.38 11.0 8.00 5.51 -90.7 TriFPrA 9.17 -1.36 10.5 9.60 5.26 -95.0 DiFPrA 9.39 -1.32 10.7 8.16 5.36 -93.3 MFPrA 9.20 -1.31 10.5 8.22 5.26 -95.1 4 PFBA 9.71 -1.80 11.5 11.7 5.76 -86.8</td><td>No. carbons Substrate^a (eV) IP (eV) (eV) (eV) EA (eV) (Debye) (Debye) (Debye) (eV) η (eV) (meV⁻¹) (eV) Σ (eV) (meV⁻¹) (eV) 2 TFA 9.73 -2.10 11.8 6.19 5.92 -84.5 -3.812 DFA 9.48 -1.37 10.9 6.50 5.43 -92.2 -4.054 MFA 9.27 -1.35 10.6 6.42 5.31 -94.2 -3.960 3 PFPrA 9.72 -1.79 11.5 8.47 5.76 -86.9 -3.964 2H-PFPrA 9.49 -1.38 10.9 9.01 5.44 -92.0 -4.055 3H-PFPrA 9.64 -1.38 11.0 8.00 5.51 -90.7 -4.128 TriFPrA 9.17 -1.36 10.5 9.60 5.26 -95.0 -3.907 MFPrA 9.20 -1.31 10.5 8.22 5.26 -95.1 -3.949 4 PFBA 9.71 -1.80 11.5 11.7 5.</td></td<>	No. carbons Substrate ^a (eV) IP (eV) (eV) (eV) EA HOMO— (Debye) (eV) (eV) η (eV) (eV) (meV ⁻¹) S (meV ⁻¹) 2 TFA 9.73 -2.10 11.8 6.19 5.92 -84.5 DFA 9.48 -1.37 10.9 6.50 5.43 -92.2 MFA 9.27 -1.35 10.6 6.42 5.31 -94.2 3 PFPrA 9.72 -1.79 11.5 8.47 5.76 -86.9 2H-PFPrA 9.49 -1.38 10.9 9.01 5.44 -92.0 3H-PFPrA 9.64 -1.38 11.0 8.00 5.51 -90.7 TriFPrA 9.17 -1.36 10.5 9.60 5.26 -95.0 DiFPrA 9.39 -1.32 10.7 8.16 5.36 -93.3 MFPrA 9.20 -1.31 10.5 8.22 5.26 -95.1 4 PFBA 9.71 -1.80 11.5 11.7 5.76 -86.8	No. carbons Substrate ^a (eV) IP (eV) (eV) (eV) EA (eV) (Debye) (Debye) (Debye) (eV) η (eV) (meV ⁻¹) (eV) Σ (eV) (meV ⁻¹) (eV) 2 TFA 9.73 -2.10 11.8 6.19 5.92 -84.5 -3.812 DFA 9.48 -1.37 10.9 6.50 5.43 -92.2 -4.054 MFA 9.27 -1.35 10.6 6.42 5.31 -94.2 -3.960 3 PFPrA 9.72 -1.79 11.5 8.47 5.76 -86.9 -3.964 2H-PFPrA 9.49 -1.38 10.9 9.01 5.44 -92.0 -4.055 3H-PFPrA 9.64 -1.38 11.0 8.00 5.51 -90.7 -4.128 TriFPrA 9.17 -1.36 10.5 9.60 5.26 -95.0 -3.907 MFPrA 9.20 -1.31 10.5 8.22 5.26 -95.1 -3.949 4 PFBA 9.71 -1.80 11.5 11.7 5.

^aFull names and structures of individual fluorocarboxylates provided in Table 1.

S3.6 Bond dissociation energy and reduction potential values.

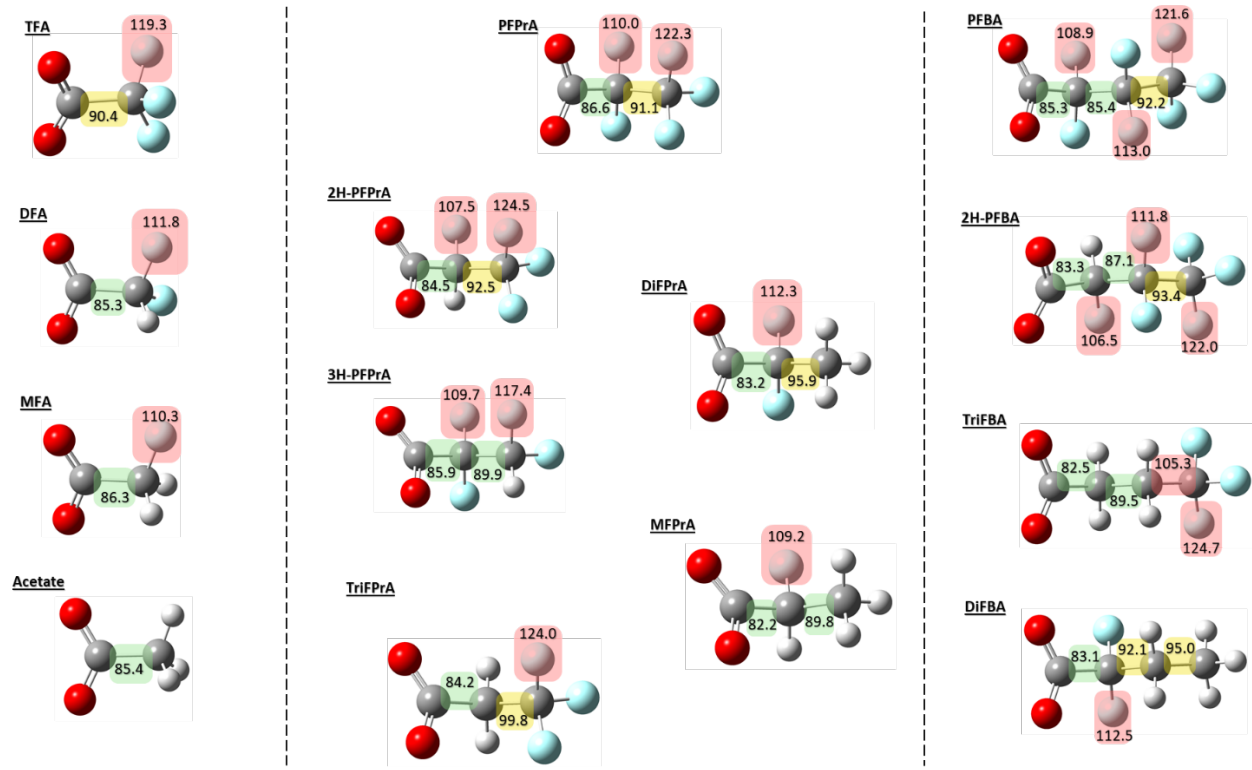


Figure S8*. Bond dissociation energies for each unique C-C and C-F bond in the fluorocarboxylate structures. Values provided in kcal/mol and are separated by two carbon (left), three carbon (middle), and four carbon (right) compounds. Bonds highlighted in red depict strong bonds that are relatively hard to break (≥ 100 kcal/mol), while yellow and green depict moderate (90–100 kca/mol) and weak (< 90 kcal/mol) bonds, respectively. *Red atoms = oxygen; blue = fluorine; grey = hydrogen.

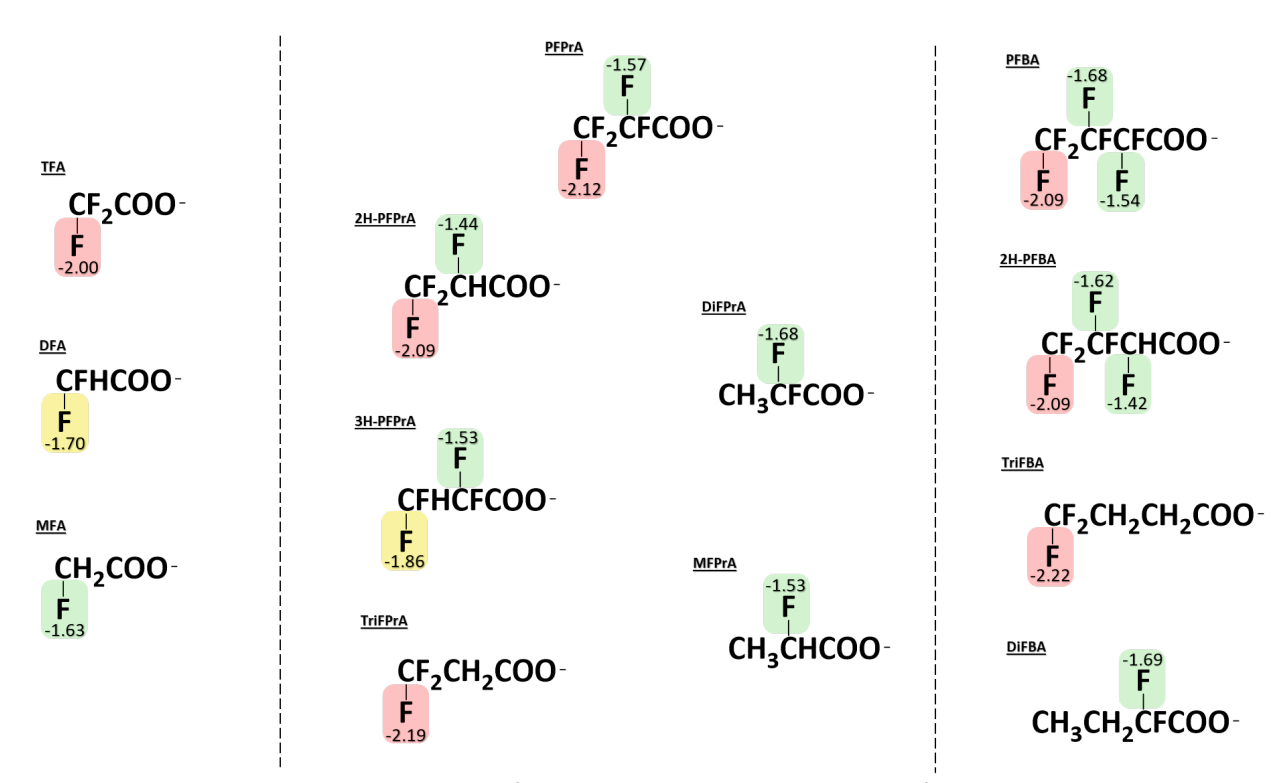


Figure S9. Reduction potentials in volts for each unique C-F bond. As before, these are separated by four, three, and two carbon compounds. Values in red represent bonds that are relatively hard to reduce (≥ 2 V), while yellow and green depict moderately (1.7–1.9 V) and easily (< 1.7 V) reducible bonds, respectively.

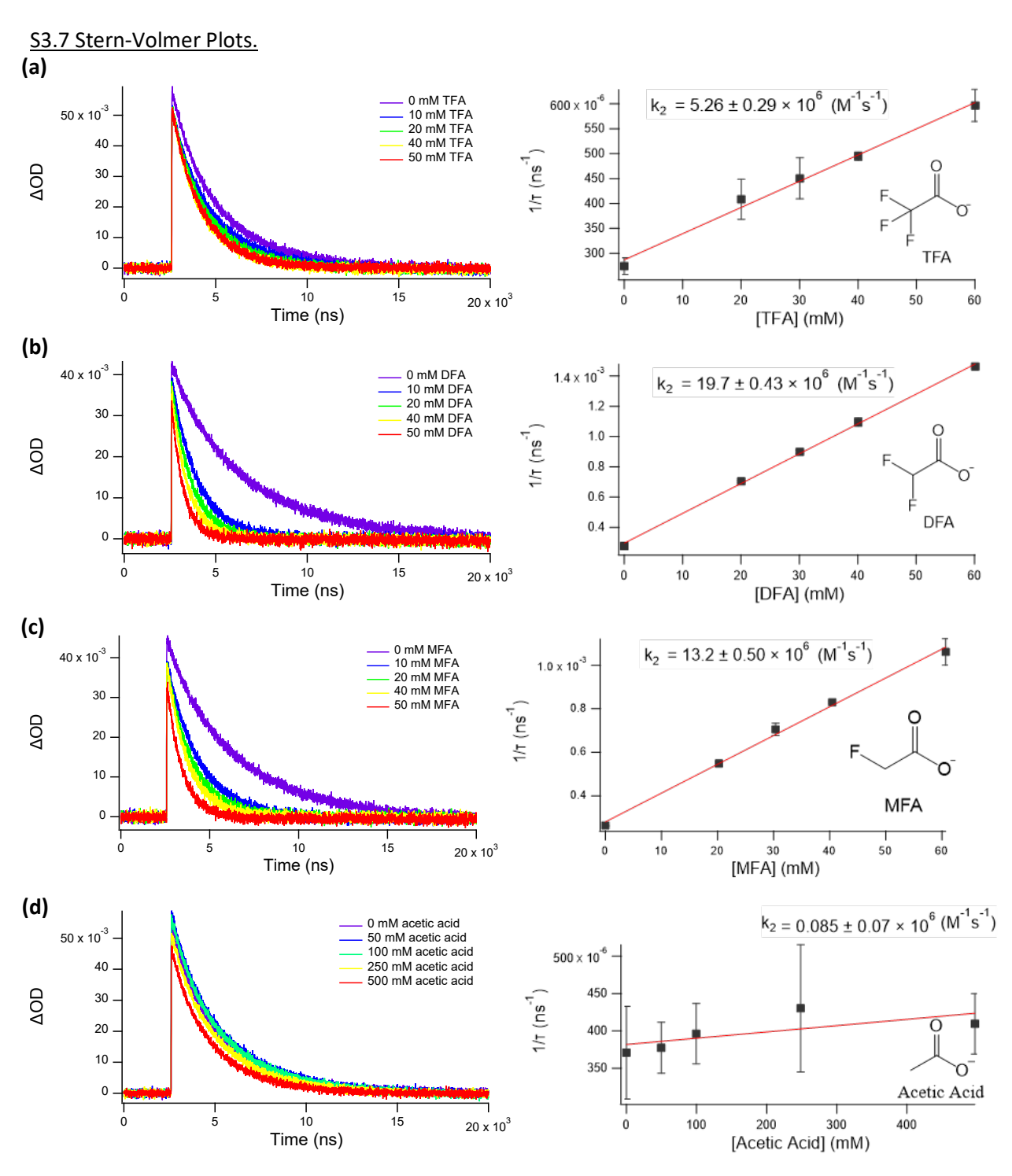


Figure S10. (Left) Transient absorbance traces depicting the decay of the characteristic 690 nm e_{aq}^- peak after photolyzing K₄Fe(CN)₆ with 254 or 266 nm light (specified in **Table 1**). (Right) Corresponding Stern-Volmer plots. Error bars represent one standard deviation, and uncertainties of the k_2 values represent standard errors of the regression-derived slope values using the *linest* function in Excel. Solution conditions the same as **Figure 1**.

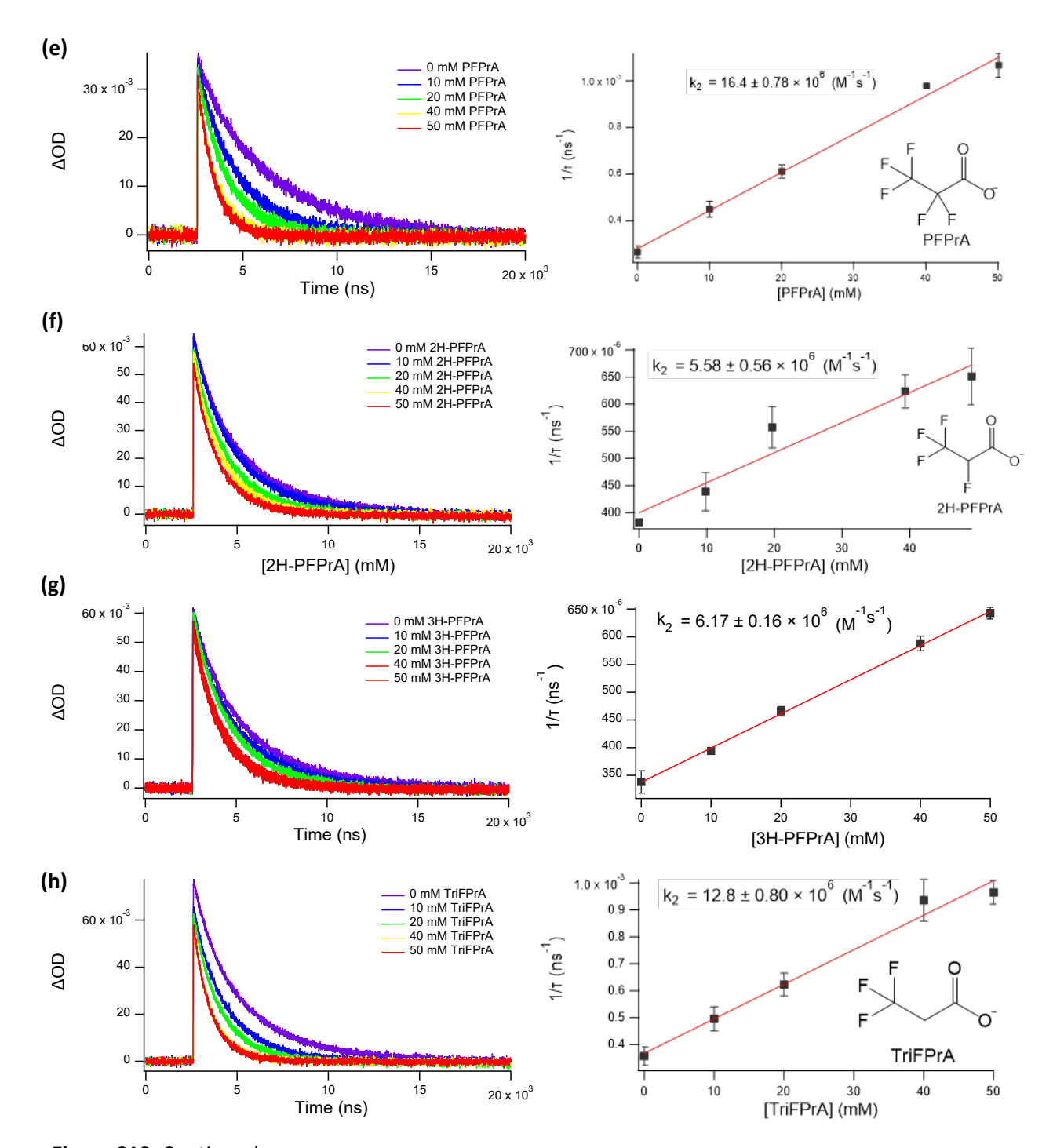


Figure S10. Continued.

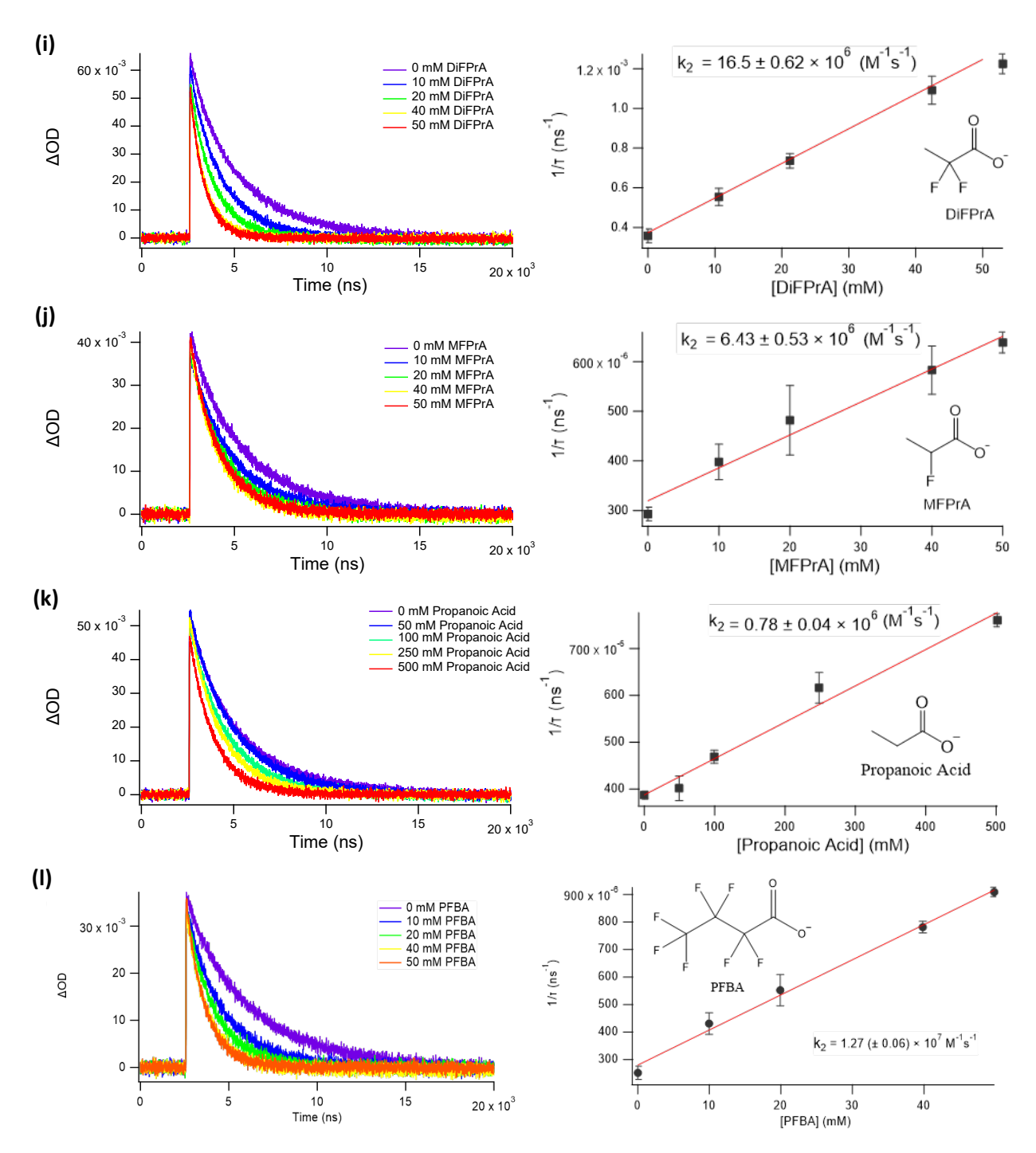


Figure S10. Continued.

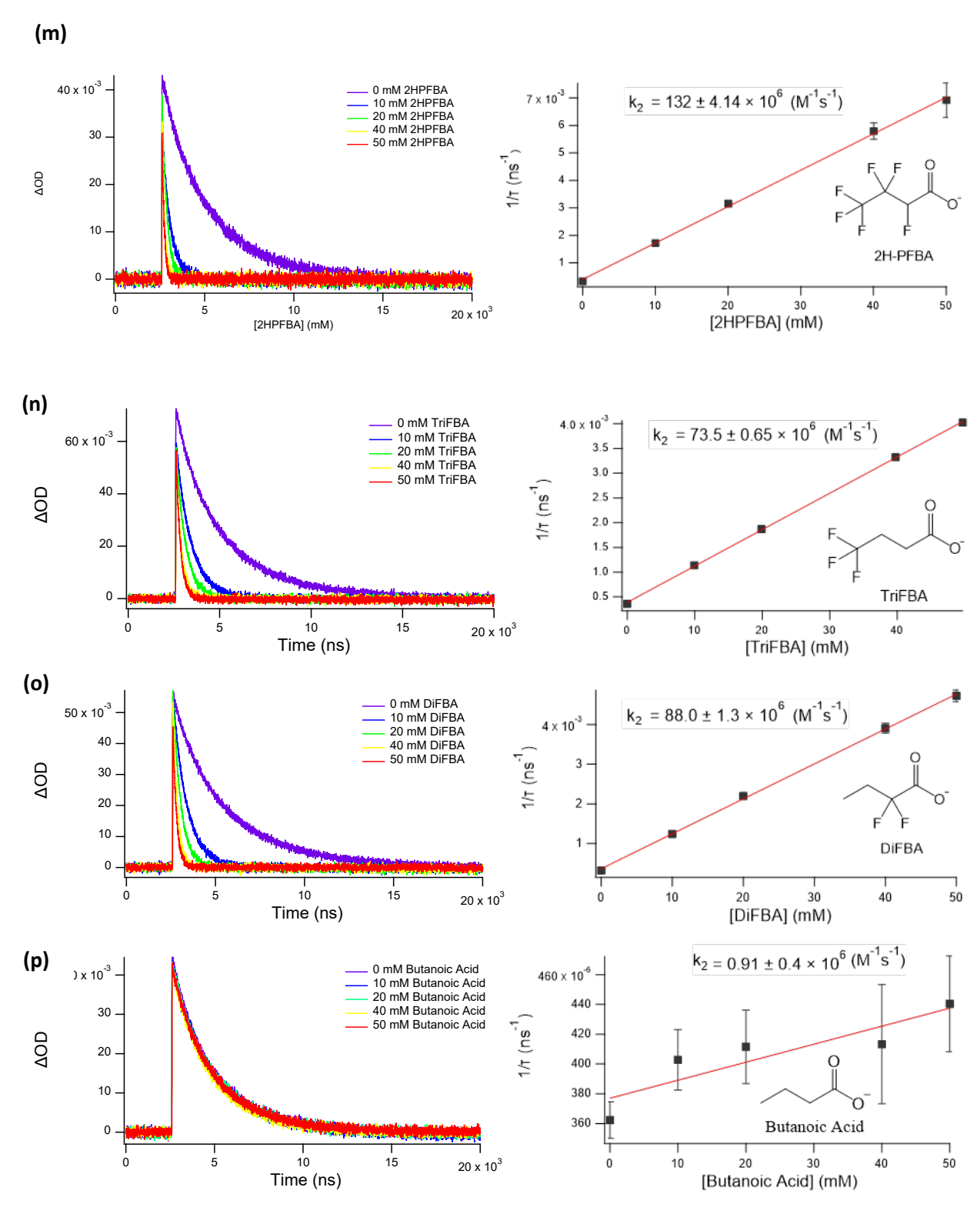


Figure S10. Continued.

S3.8 Optimized ω B97-XD/aug-cc-pVDZ geometries in SMD.

Trifluoroacetate	e (TFA) - Charge = -1 Mult	iplicity = 1		
С	0	1.234438	-0.93491	0.222272
С	0	-0.24679	-0.46595	0.082474
0	0	-0.88065	-0.91519	-0.89149
0	0	-0.61467	0.316403	0.984358
F	0	1.435651	-1.57203	1.398435
F	0	1.62863	-1.77643	-0.74985
F	0	2.083883	0.117728	0.198474
Difluoroacetate	(DFA) - Charge = -1 Mult	iplicity = 1		
С	0	-0.52891	0.005426	-0.02025
С	0	1.015214	0.020126	0.006813
0	0	1.595948	1.127418	0.024751
0	0	1.528925	-1.12561	-0.00612
F	0	-0.99266	-0.62892	1.115282
F	0	-1.0632	1.267218	0.006056
Н	0	-0.93386	-0.52063	-0.89278
Monofluoroace	tate (MFA) - Charge = -1	Multiplicity = 1		
С	0	-0.52619	0.024879	0.019179
С	0	0.99792	-0.01317	0.008869
0	0	1.52959	0.909914	-0.66922
0	0	1.597179	-0.91456	0.643613
F	0	-1.08484	-1.0149	0.782532
Н	0	-0.90714	-0.07734	-1.00478
Н	0	-0.87131	0.971909	0.452596
D. (1)	(DED A) Charac	a na liteliteti – a		
	onate (PFPrA) - Charge =	-1 Multiplicity = 1 1.205033	0.74007	0 211016
C C	0 0	-0.33842	-0.74987 -0.48718	0.211816 0.172599
0	0			-0.96411
0	0	-0.85006 -0.86515	-0.52215 -0.25411	1.278502
C	0	-0.86515 2.04887	0.532603	0.034226
F		1.783267	1.411424	1.009862
F	0	1.784928	1.411424	-1.14228
F	0	1.784928 3.35936		
F	0		0.251931	0.073845
	0	1.583924	-1.30826	1.393455
F	0	1.584257	-1.6082	-0.77442

2,3,3,3-tetrafluoi	opropanoate (2H-PFP	r A) - Charge = -1 Multi	plicity = 1	
С	0	-0.05633	0.467708	0.05026
С	0	-1.44819	-0.19609	-0.09598
0	0	-2.06421	-0.46826	0.956367
0	0	-1.81863	-0.38188	-1.28036
С	0	1.079501	-0.43635	-0.42477
F	0	1.022994	-1.66011	0.141651
F	0	2.280098	0.086597	-0.10239
F	0	0.224642	0.768414	1.377217
Н	0	-0.0172	1.397823	-0.52926
F	0	1.065946	-0.60619	-1.75607
2,2,3,3-tetrafluoi	opropanoate (3H-PFP)	r A) - Charge = -1 Multi	plicity = 1	
С	0	0.203281	0.546623	-0.15832
С	0	1.537581	-0.24277	0.002137
0	0	2.254501	-0.36125	-1.0105
0	0	1.720941	-0.68157	1.160303
С	0	-1.02983	-0.31419	0.13477
F	0	-1.06834	-1.33259	-0.77536
F	0	-2.15814	0.431908	-0.04524
F	0	0.184361	1.598112	0.723359
F	0	0.073317	1.083998	-1.40341
Н	0	-1.02612	-0.72673	1.148414
3,3,3-trifluoropro	panoate (TriFPrA) - Ch	narge = -1 Multiplicity	= 1	
С	0	0.226878	-0.36047	-0.8538
С	0	1.553048	-0.00847	-0.15147
0	0	2.29129	-0.97205	0.183684
0	0	1.805186	1.212509	0.024769
С	0	-0.97888	-0.03567	-0.01586
Н	0	0.181812	-1.43225	-1.07161
Н	0	0.135106	0.203774	-1.78951
F	0	-1.17465	1.288457	0.1749
F	0	-0.9164	-0.59124	1.220751
F	0	-2.11958	-0.50464	-0.58244

2,2-difluoropropa	noate (DiFPrA) - Cha	rge = -1 Multiplicity = 1		
С	0	-0.02609	0.450715	0.032736
С	0	-1.4397	-0.16798	-0.14484
0	0	-1.91251	-0.76956	0.84741
0	0	-1.9475	-0.0484	-1.28493
С	0	1.091137	-0.46187	-0.39441
F	0	0.045886	1.639486	-0.67492
F	0	0.157178	0.824016	1.352303
Н	0	0.966907	-0.71993	-1.45219
Н	0	1.060115	-1.37936	0.205044
Н	0	2.053666	0.042044	-0.24611
2-fluoronronanoa	te (MFPrA) - Charge	= -1 Multiplicity = 1		
С	0	-0.51873	0.031088	0.050003
C	0	1.013141	0.024002	-0.0342
0	0	1.643463	1.088706	0.182755
0	0	1.518282	-1.09382	-0.3334
C	0	-1.17574	-0.15105	-1.30255
F	0	-0.97282	1.253834	0.60252
Н	0	-0.89073	-1.12383	-1.72106
Н	0	-0.85828	0.638867	-1.99639
Н	0	-2.26739	-0.1234	-1.19842
Н	0	-0.83548	-0.74899	0.754314
Perfluorobutanoa	i te (PFBA) - Charge =	-1 Multiplicity = 1		
С	0	1.208096054	-0.781809703	0.196053419
F	0	1.517274933	-1.35556174	1.391878265
F	0	1.590582932	-1.656099098	-0.773648585
С	0	-0.3286993	-0.476047966	0.11737567
0	0	-0.880643606	-0.746938315	-0.965607384
0	0	-0.80821861	0.017299202	1.15848437
С	0	2.072904029	0.498828401	0.048079972
F	0	1.614303295	1.217868162	-1.004596443
F	0	1.94482022	1.250485138	1.162505324
С	0	3.593958346	0.27380965	-0.185375298
F	0	3.824018655	-0.245596332	-1.392681737
F	0	4.23038546	1.448515177	-0.108490102
F	0	4.103916593	-0.542946576	0.74099653

2H-perfluorob	utanoate (2H-PFBA) - Charg	ge = -1 Multiplicity	<i>y</i> = 1	
С	0	-0.84234	-0.47549	0.210621
F	0	-0.59213	-0.68351	1.563073
С	0	-2.23203	0.174022	-0.01269
0	0	-2.60264	0.211498	-1.21022
0	0	-2.8425	0.582178	0.99809
С	0	0.286784	0.41215	-0.32106
F	0	0.254118	0.440662	-1.67669
F	0	0.147693	1.694075	0.118715
С	0	1.720951	-0.03859	0.076291
F	0	1.8921	-1.34107	-0.18611
F	0	2.625623	0.651501	-0.63153
F	0	1.965253	0.171985	1.371803
Н	0	-0.79732	-1.44543	-0.29756
4,4,4-trifluoro	butanoate (TriFBA) - Charge	e = -1 Multiplicity	= 1	
С	0	-2.29251	0.028336	-0.02491
С	0	-0.88024	-0.54787	0.097631
Н	0	-0.48773	-0.33903	1.099356
Н	0	-0.91773	-1.63288	-0.05583
С	0	0.023663	0.094019	-0.95867
Н	0	-0.352	-0.10426	-1.97008
Н	0	0.082455	1.180739	-0.81858
С	0	1.433531	-0.42433	-0.91275
0	0	-3.07791	-0.51978	-0.85048
0	0	-2.58045	1.031662	0.688286
F	0	2.217913	0.15904	-1.85259
F	0	1.51417	-1.76032	-1.13088
F	0	2.042212	-0.20115	0.278124
2,2-difluorobu	tanoate (DiFBA) - Charge =	-1 Multiplicity = 1		
С	0	-1.25807	0.035195	0.036068
С	0	0.16275	-0.56529	0.211972
С	0	1.264904	0.388302	-0.1942
Н	0	1.07358	0.67041	-1.23814
Н	0	1.143395	1.29362	0.414889
С	0	2.667955	-0.18745	-0.03549
Н	0	2.809669	-1.07673	-0.66243
Н	0	3.407066	0.563093	-0.34174
Н	0	2.874094	-0.45967	1.007365
0	0	-1.81701	-0.17167	-1.06664
0	0	-1.69018	0.712012	0.999479
F	0	0.261153	-1.74118	-0.51052
F	0	0.333858	-0.95751	1.529062

S4. References Cited in Supporting Information

- Bentel, M.J., Yu, Y., Xu, L., Li, Z., Wong, B.M., Men, Y., Liu, J., 2019. Defluorination of Per- and Polyfluoroalkyl Substances (PFASs) with Hydrated Electrons: Structural Dependence and Implications to PFAS Remediation and Management. Environ. Sci. Technol. 53, 3718–3728. https://doi.org/10.1021/acs.est.8b06648
- Cárdenas-Jirón, G.I., Gutiérrez-Oliva, S., Melin, J., Toro-Labbé, A., 1997. Relations between Potential Energy, Electronic Chemical Potential, and Hardness Profiles. J. Phys. Chem. A 101, 4621–4627. https://doi.org/10.1021/jp9638705
- Chen, L.-Q., 2019. Chemical potential and Gibbs free energy. MRS Bull. 44, 520–523. https://doi.org/10.1557/mrs.2019.162
- Gu, Y., Liu, T., Zhang, Q., Dong, W., 2017. Efficient decomposition of perfluorooctanoic acid by a high photon flux UV/sulfite process: Kinetics and associated toxicity. Chemical Engineering Journal 326, 1125–1133. https://doi.org/10.1016/j.cej.2017.05.156
- Hart, E.J., 1969. The Hydrated Electron, in: Survey of Progress in Chemistry. Elsevier, pp. 129–184. https://doi.org/10.1016/B978-0-12-395706-1.50010-8
- Huang, L., Dong, W., Hou, H., 2007. Investigation of the reactivity of hydrated electron toward perfluorinated carboxylates by laser flash photolysis. Chemical Physics Letters 436, 124–128. https://doi.org/10.1016/j.cplett.2007.01.037
- Li, X., Fang, J., Liu, G., Zhang, S., Pan, B., Ma, J., 2014. Kinetics and efficiency of the hydrated electron-induced dehalogenation by the sulfite/UV process. Water Research 62, 220–228. https://doi.org/10.1016/j.watres.2014.05.051
- Li, X., Ma, J., Liu, G., Fang, J., Yue, S., Guan, Y., Chen, L., Liu, X., 2012. Efficient Reductive Dechlorination of Monochloroacetic Acid by Sulfite/UV Process. Environ. Sci. Technol. 46, 7342–7349. https://doi.org/10.1021/es3008535
- Parr, R.G., Szentpály, L. v., Liu, S., 1999. Electrophilicity Index. J. Am. Chem. Soc. 121, 1922–1924. https://doi.org/10.1021/ja983494x
- Pearson, R.G., 1966. Acids and Bases. Science 151, 172–177. https://doi.org/10.1126/science.151.3707.172
- Song, Z., Tang, H., Wang, N., Zhu, L., 2013. Reductive defluorination of perfluorooctanoic acid by hydrated electrons in a sulfite-mediated UV photochemical system. Journal of Hazardous Materials 262, 332–338. https://doi.org/10.1016/j.jhazmat.2013.08.059
- Tenorio, R., Liu, J., Xiao, X., Maizel, A., Higgins, C.P., Schaefer, C.E., Strathmann, T.J., 2020. Destruction of Per- and Polyfluoroalkyl Substances (PFASs) in Aqueous Film-Forming Foam (AFFF) with UV-Sulfite Photoreductive Treatment. Environ. Sci. Technol. 54, 6957–6967. https://doi.org/10.1021/acs.est.0c00961
- Yu, K., Li, X., Chen, L., Fang, J., Chen, H., Li, Q., Chi, N., Ma, J., 2018. Mechanism and efficiency of contaminant reduction by hydrated electron in the sulfite/iodide/UV process. Water Research 129, 357–364. https://doi.org/10.1016/j.watres.2017.11.030